POLITECNICO DI TORINO

Master's Degree in Mechanical engineering

Master's Degree Thesis

Experimental and numerical investigation on the quasi-static and dynamic response of hybrid glass/flax composite laminates

Supervisors

Prof. Raffaele CIARDIELLO

Prof. Alberto CIAMPAGLIA

Prof. Davide Salvatore PAOLINO

Candidate

Samuel BARBAGLIA

1st APRIL 2025

Abstract

Composite materials consist of a matrix and one or more reinforcements, combining to form a material that enhances the properties of both components. This thesis focuses on long fiber-reinforced materials, which are widely used in various industrial sectors such as aerospace, automotive, energy, marine, and sports and leisure due to their high mechanical properties and reduced weight compared to traditional materials like aluminum alloys and steel.
These properties make fiber-reinforced composite materials significant for sustainable applications, such as reducing fuel consumption in the automotive and aerospace industries and decreasing inertia and energy dissipation in wind turbines.
To enhance the sustainability of these materials, research was conducted on the mechanical properties of a hybrid composite made with commercial materials. Four symmetric and balanced laminates composed of flax fiber and E-glass fiber, along with two additional plates each containing only one type of reinforcement, were manufactured.
Flax fiber has emerged as a highly promising reinforcement for sustainable composite materials due to its superior mechanical properties compared to most other sustainable fibers studied to date.
To further increase the sustainability of the composite, an epoxy resin containing a percentage of bio-based raw materials was used.
An experimental campaign was conducted to obtain the principal mechanical properties of each plate, followed by a finite element (FE) analysis. The goal of this analysis was to identify the best material model to describe the laminates composed of a single fiber type and to determine the optimal parameters for using these material models to accurately reproduce the mechanical properties of the hybrid laminates.
Finally, an evaluation of the trade-off between mechanical properties and sustainability was conducted to explore potential scenarios where a hybrid composite could be used instead of an exclusively E-glass fabric reinforced material.

Acknowledgements

Scrivo questi ringraziamenti come ultima cosa della tesi, poco prima di inviare la versione definitiva, di modo da essere il più spontaneo possibile.

Questo percorso di laurea è stato incredibile, la mia vita mi è esplosa in mano e non sarebbe mai tato possibile senza tutto ciò che è successo in questi anni, ed è per questo che ci tengo a ringraziare tutte le persone che mi hanno insegnato qualcosa della vita.

Partendo dagli amici conosciuti a lezione, come piace chiamarci a noi "Repeatability", un gruppo di persone ambiziosissime con cui ho passato tantissimo tempo tra studio e nelle pochissime serate che il Politecnico ci ha concesso e con alcuni dei quali ho anche passato tantissime ore in tutte le sale studio possibili ed immaginabili di Torino, mi aggancio per ringraziare anche tutti gli altri ragazzi con cui ho passato queste ore in sala studio e con i quali ho fatto un sacco di pause caffettino.

È importantissimo ringraziare i ragazzi conosciuti a Biella, Sara, Gaia, Gabri, Fede e Ste, i quali sono stati i miei coinquilini una volta trasferiti a Torino, gli unici con i quali ho condiviso l'intero percorso.

Non posso dimenticare tutti i ragazzi del Team, con i quali ho passato gran parte della mia laurea magistrale, ho imparato ad essere un ingegnere e con i quali abbiamo fatto cose incredibili e vissuto avventure pazzesche, tra test, produzione di prototipi, orari improponibili, notti insonni ed il Nevada, che sarà probabilmente la settimana più bella della mia vita.

Un ringraziamento alla compagnia di Boca, persone che mi hanno accompagnato in tutta la mia vita e non solo negli anni universitari, anche se ci si vede sempre di meno non dimenticherò mai tutto il tempo passato assieme.

Ultimo ma non per importanza la mia famiglia, che mi ha supportato e sopportato in tutti questi anni, mi hanno permesso di terminare gli studi facendo sacrifici inimmaginabili e che hanno condiviso gli sforzi e la sofferenza di questi anni di studio.

Infine, vorrei ringraziare il Politecnico di Torino, come ente, che mi ha aiutato a crescere ed ho imparato tantissime cose che utilizzerò e già sto utilizzando nella mia vita da adulto e non sto parlando di conoscenze tecniche, almeno non solo, ma

anche di come comportarsi professionalmente e di come comportarmi in ambito professionale e di come costruirmi una carriera.

"Ce l'abbiamo fatta Pa! "

Table of Contents

List of Tables

List of Figures

Acronyms

CFRP
Carbon Fiber Reinforced Polymer

DIC
Digital Image Correlation

FEA
Finite Element Analysis

FEM
Finite Element Method

FRP
Fiber Reinforced Polymer

GFRP
Glass Fiber Reinforced Polymer

LSTC
Livermore Software Technology Corporation

PA
Polyamides

PAN
Polyacrylonitrile

PEI
Polyetherimide

PEAK

Polyetherketoneketone

PEEK

Polyetherketoneketone

PEKK

Polyetherketoneketone

PP

Polypropylene

PSU

Polysulfone

TDS

Technical Data Sheet

UTM

Universal Testing Machine

Chapter 1

Introduction

Composite materials are a family of heterogeneous materials composed of a matrix and one or more reinforcements, whose combined properties are enhanced compared to those of the individual phases. Composite materials can be either natural or artificial. A natural example of a composite material is wood, where the matrix is composed of lignin, while the cellulose fibers serve as the reinforcements.

The first man-made composites were created by the Egyptians and Mesopotamian who made bricks using *"a mixture of mud and straw to create strong and durable buildings"[1].*

To speak about composites as we understand them today, it is necessary to wait until the 1900s with the chemical revolution. In the early 1900s, some resins were developed, but it was in 1935 that *"Owens Corning introduced the first glass fiber, fiberglass. ... This is the first Fiber Reinforced Polymers (FRP) industry as we know it today."[1].*

The first major use of GFRP (Glass Fiber Reinforced Polymer) was during World War II, when this material was developed for its mechanical properties and lightweight nature, but also because it is transparent to radio frequencies, making it ideal for covering electronic radar equipment.

After World War II, composite materials became a focus of interest in the space race due to their lightweight properties. In the 1970s, both aramid fibers and carbon fibers were introduced to the market, leading to the development of composite materials as we know them today.

These materials have incredible mechanical properties, which are even more impressive when compared to the weight savings achieved by producing components with reinforced polymer composites instead of conventional materials like steel or aluminum. However, they present a significant challenge: their carbon footprint.

The production of fibers such as glass fibers, carbon fibers and aramid fibers is energy-intensive, both for manufacturing the fibers themselves and their precursors. This, combined with the environmental impact of the polymers used, typically

thermosets like epoxy resin, makes these materials quite problematic in terms of pollution and environmental sustainability.

In recent years, there has been a strong push toward using natural fibers to significantly reduce the carbon footprint of composite reinforcements. This has led to the commercialization of various natural fiber-based products. Among them, flax fibers are the most widely used today due to their favorable mechanical properties and high energy absorption before failure.

Additionally, bio-based resins have been developed, resulting in epoxy resins that incorporate a substantial amount of plant-based raw materials in their formulation.

During this thesis work, research was conducted on a composite made of flax fibers and bio-based epoxy resin. Some attempts were made to mix layers of flax fibers with layers of glass fibers, resulting in hybrid composites. The stacking sequence of the composite was modified, producing four symmetric plates with different glass and flax stacking sequences.

1.1 Constituents

Nowadays the world of composite materials increased in dimensions, with different type of approaches used to increased matrices properties. We can divide composite materials in two different families, particulate reinforced materials and fibrous reinforced materials.

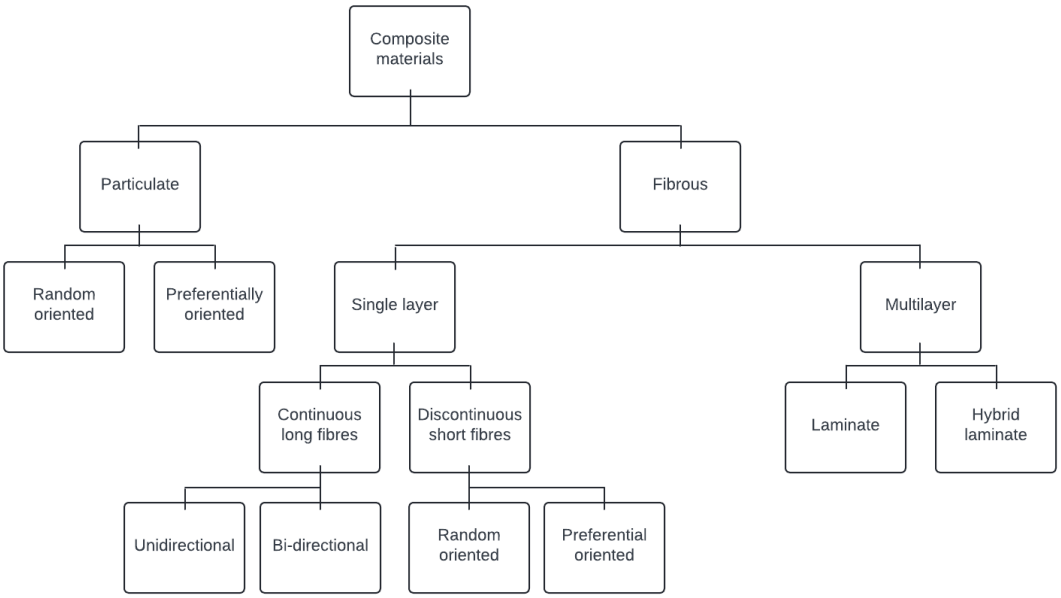

Figure 1.1: Composite materials classification

1.1.1 Particulate

Particle reinforced materials are usually reinforced with metallic or ceramic particles. The effect of this particles are usually related to a stiffness increment but they can also be added for modifying the electrical properties. Sometimes it can be used a mixture of particles into a matrix that is then used with long fibers reinforcements in order to increase the mechanical properties of the matrix and having them more close to the one of the reinforcements.

1.1.2 Fibers

In many cases, when mechanical properties are the most relevant aspect, reinforcement are made of fibers. The mechanical properties of the material are enhanced because the small section of the fibers, that decrease the probability of having a defect inside the material. A fiber has a high length-to-diameter ratio and the diameter has the same order of magnitude of a crystal.

Commonly used fibers

There are two type of reinforcement that are the most used all over the world. Glass fibers are for sure the most used, they are cheaper than other fibers available on the market and they guarantee high strength and good mechanical properties. It is possible to find them in two forms, long and short fibers. These fibers are chemically made of Silicon dioxide (SiO_2). There are two type of Glass fibers, E-Glass fibers and S-Glass fibers, that are divided using the purity of the glass used. E-Glass fibers are the first fibers appeared on the market, the letter "E" stand for electrical, in fact they were used in the electrical fields such as insulators. S-Glass fibers are produced in a lower quantity and they are used for their enhanced mechanical properties; letter "S" stands for structural, in fact those fibers are used also for structural components purposes.

The other most used fibers are the Carbon fiber reinforcements. They are widely used because of their good mechanical properties and their lightweight. They are more expensive if compared with Glass fibers, for this reason in many occasions Glass fibers are preferred.

If the percentage of carbon inside the fiber is around $80 - 95\%$, they are called Carbon fibers, while if the percentage is increased till reaching an amount of 99%, they are called Graphite fibers. Graphite fibers have higher Young modulus, but a lower elongation at breakage if compared with Carbon fibers.

The high cost of these fibers is due to the production process. In fact for Carbon fibers it is necessary to heat the precursor till 1500°, while for graphite fibers an extra eating at temperatures around 3000°C is necessary. Also the precursor of the

fibers is different, for high strength fibers a Polyacrylonitrile (PAN) fiber is used, while for high modulus fibers a Pitch precursor is used.

Natural fibers

During last years the problems related with the derivation of the reinforcements from fossil sources are becoming more and more evident. For this reason many researches about limiting their usage are conducted world wide.

The most used fiber worldwide are Glass fibers and Carbon fibers, that have an high carbon footprint during their entire lifecycle. For this reason the use of natural fibers is increasing in the last years, to limit the use of classical reinforcements. We can divide natural fibers in two different groups, plant fibers, mainly composed by cellulose and animal fibers, which have protein as major component.

We can subdivide those two groups in other subgroups[2]. Plant fiber can be collected into eight different fiber types: Bast fibers (collected from the skin and bast around the plants stem); Leaf fibers (collected from leaves); Seed fibers (collected from seeds and seed cases); Grass fibers; Core fibers (collected from the stalks of the plants); Wood pulp fibers; Root fibers; Fruit fibers. Animal fibers can be divided in other three subgroups: Fibers of animal hair (from hairy mammals and animals); Avian fibers (from the feathers of birds); Silk fibers (from the dried saliva of bugs) Those fibers have many benefits with respect to synthetic fibers, such as a lower carbon footprint, higher renovability, higher heat and sound insulation and higher damping properties and they are also easier to use due to their non toxicity and the capability of being manipulated without irritate the skin. On the other hand, their mechanical properties are lower if compared with synthetic fibers, have lower durability both in fiber form and when the composite material is produced, their mechanical properties and quality can varies for many reasons, starting from the environmental condition where the precursor grow (higher influence for plant fibers) but also during the transportation and stocking condition of the fibers before being produced. Another disadvantage is the limited thermal resistance that can also influence the processing parameters of those fibers.

1.1.3 Flax fiber

Flax fibers are the most prevalent natural fibers on the market. Their development began a few years ago. The energy cost of producing these fibers can be as low as one-fifth of the total energy needed to produce traditional fibers and the end-of-life footprint of those fibers are many times lower than other fibers. Of course those fibers cannot be recycled if laminated with thermosets matrices, because while burning away the matrix, also the fibers are degraded.

Flax fibers have some drawbacks. The first one is that their mechanical properties

are influenced from their harvesting period. Another one, always correlated with their growth, is that in case of bad weather years or in case of natural events that ruin the harvest, the capability from the industry to provide the amount of material required can be compromised, leading to supply chain disruptions and potential increases in material costs. Additionally, natural fibers can exhibit variability in quality due to differences in soil conditions, climate, and other environmental factors during growth. This inconsistency can result in variations in the final product's performance and durability, making it challenging to maintain standardized quality levels in industrial applications.

Flax fiber fabrics production

Flax fibers fabrics are produced with flax fibers, that are bio fibers with good mechanical properties. For this reason, flax fibers fabrics are one of the most technical textiles used nowadays for mechanical applications and sometimes also for structural applications.

The production of flax is explained in the paper "Flax Fiber for Technical textile: a life cycle inventory"[3] The raw material to produce fibers is Flax (Linum usitatissimum), that is a plant mainly grown in western Europe. The countries that produce more flax plants are the one on the western cost such as France, Belgium and Netherlands.

The production of Flax start with the sowing of flax seeds, where for each hectare of terrain, 115 kg of seeds are planted. Sowing take place between March and April. Stems takes 100 days to reach an height of 1 meter. In July around 7000 $\frac{kg}{ha}$ of flax stems can be harvested. After harvesting, the first step is the retting, where stems are laid on the field and turn over to have an homogenized porcess on the stems. Microorganisms of the soil and the weather help this process, that's the reason why the stems are left on the field. Because this process is not controllable, it can take between two and twelve weeks in total.

After retting, stems are scutched to obtain different products like long or short fibers but also flakes and grains and other products. Only long fibers are used for high properties fibers. After being selected, long fibers are combed and spin into yarns, usually this process is done in China. From Yarns, the fabrics can be obtained using fabric looms. If the fabrics are going to be used with a matrix for a composite product, the yarn is subject to sizing deposition before being weaved.

The same paper cited before, "Flax Fiber for Technical textile: a life cycle inventory"[3], also report a summarization of the impact that Flax fibers has on the environment, reported here in table 1.1

Table 1.1: Results of the environmental impact of producing flax fiber technical textile issued from one ha of cultivated land

Impact category	Total/ha	Total/m² of technical textile	Unit
Climate change	18162	7.79	kg CO_2 eq
Ozone depletion	3.6×10^{-4}	1.55×10^{-7}	kg CFC-11 eq
Particulate matter	52	0.02	kg PM2.5 eq
Ionizing radiation	1048	0.45	kBq U235 eq
Photochemical ozone formation	87	0.04	kg NMVOC eq
Acidification	194	0.08	molc H^+ eq
Freshwater eutrophication	4.5	1.2×10^{-3}	kg P eq
Marine eutrophication	23	9.8×10^{-3}	kg N eq
Mineral, fossil & renewable resource depletion	0.48	2.1×10^{-4}	kg Sb eq

1.2 Matrices

In composite materials, matrices have a relevant role in the final performances of the material. The functions of the matrix are a lot, from transmitting the force between fibers, arresting the crack propagation between fibers to taking the fibers with the correct orientation. Polymers matrices have a huge range of usage, but a drawback in using this type of matrix is the fact that the maximum temperature at which it can work is quite low if compared with metal matrices of ceramic matrices.

These matrices family can be divided into two general groups: thermoset matrices and thermoplastics. The main difference between these two types of matrices is that thermoplastics can be melted and reformed multiple times, whereas thermosets, once the polymer has cross-linked, will burn if heated further. It is impossible to revert thermosets back to their original, uncross-linked state.

Thermosets

Thermoset matrices are the first matrices used for FRP composites materials. The most used materials of this family of polymers are:

- Epoxy Resin
- Phenolic resins
- Polyester
- Vinylester

Thermoplastics

Thermoplastics matrices are becoming more and more used in last years. Thermoplastics have the fortune that the part produced can be pressed after obtaining the first shape. Most used materials are:

- Polypropylene (PP)
- Acrylonitrile-butadiene styrene (ABS)
- Polyamides (PA)
- Polyetherketone family (PEKK, PEEK, PAEK, PEAK etc.)
- Polyetherimide (PEI)
- Polysulfone (PSU)

1.3 Composite manufacturing

Composite materials parts have to be manufactured with an addiction technology. The peculiarity of those materials is the fact that the part and the material are simultaneously created.

There are certain materials with thermoplastic matrices that can be formed after the creation of the composite, by melting and consolidating the thermoplastic matrix. However, due to the lower mechanical performance of the matrix, these materials are typically used for non-structural purposes or in cases where the load on the component is not so high.

To produce thermoset composites, it is possible to use prepregs or wet-forming.

Wet-forming processes typically used are: Hand layup, Bag molding, Filament winging, RTM, Pultrusion. On the other hand, prepregs are materials in a semi-cured form. Fibers or fabric are impregnated with resin and stored at very low temperature to slow down the curing process of the matrix.
During this experimental campaign, a thermoset bio-based resin was used, and the vacuum bag molding technique was applied. Some phases of this process are shown in the pictures 1.2. The use of the vacuum bag helps evenly distribute the matrix within the composite, resulting in a more uniform matrix distribution compared to hand layup. This also leads to a more consistent density and a reduction in defects and micro-porosity inside the material.

The final result obtained with this production methodology is not the best one that it is possible to have nowadays, in fact epoxy composite parts are cured in autoclaves controlling both temperature and pressure, in this way micro porosity defects percentage is decreased and prepreg fibers are used to better control the matrix distribution.

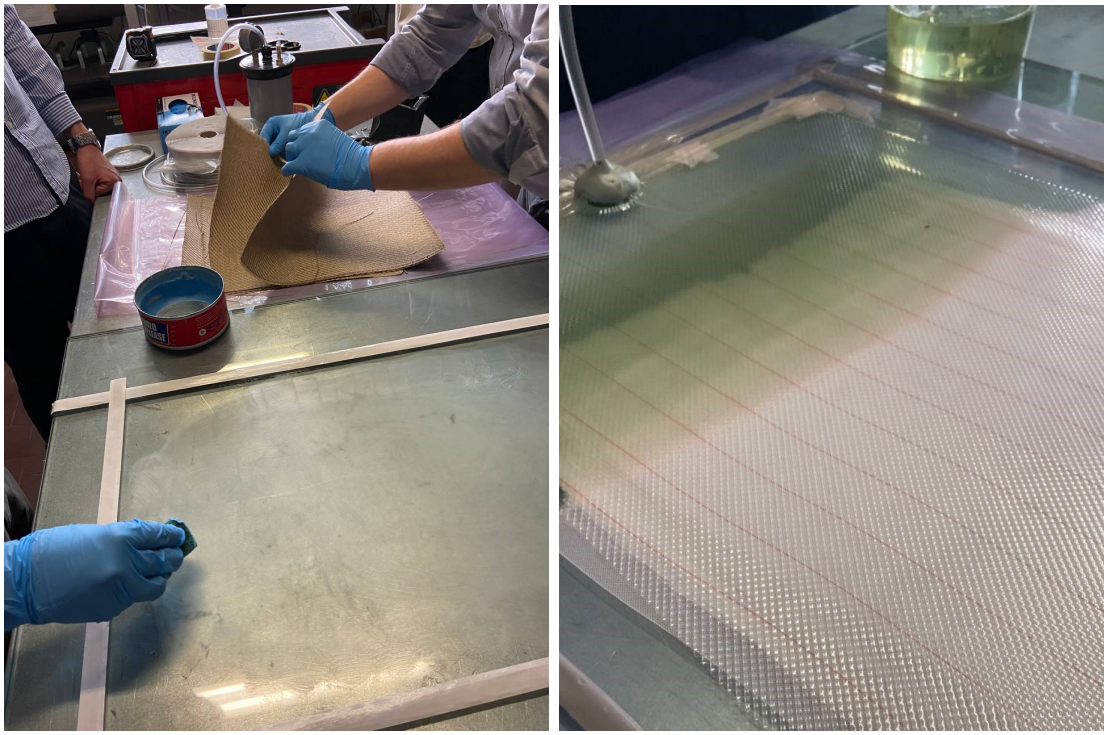

(a) Mold waxing and plies preparation **(b)** Resin infusion

Figure 1.2: Vacuum bag infusion preparation of an hybrid glass/flax/epoxy composite

1.4 Mechanics of fiber reinforced composites

The fracture in composites can occur in many ways, depending on how the load is applied. To evaluate all the possible modes it is useful to start studying the failure modes inside a single lamina.

Lamina Failure

The laminate strength is mainly influenced from the single lamina strength[4]. During the years many failure theories have been purposed, each of them is based in individuating the stresses that occur in the local axes and then check if the lamina is failed by using the strength parameters. The main directions on the lamina are reported in figure 1.3.

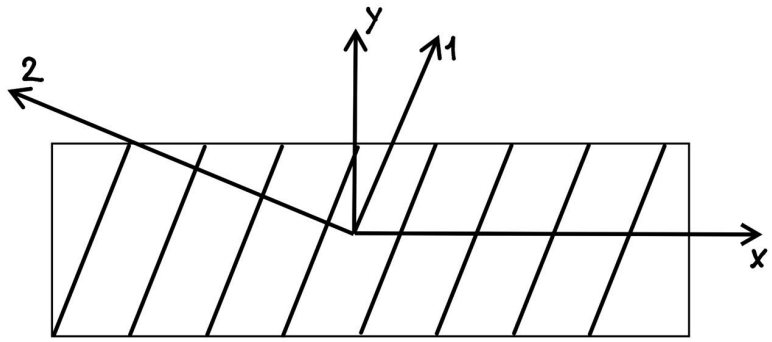

Figure 1.3: Representation of the main directions in an off-axis unidirectional lamina

Maximum stress theory This theory assume that the lamina failure occur if one of the five stresses reach or exceeds the corresponding ultimate strength.
For an unidirectional lamina, the five main strength parameters are:

- Longitudinal tensile strength σ_{Ltu}
- Transversal tensile strength σ_{Ttu}
- Longitudinal compressive strength σ_{Lcu}
- Tensile compressive strength σ_{Tcu}
- In-plane shear strength τ_u

The subsequent batch of equations is used to compare the stresses. All the inequality have to be

$$\begin{cases} -\sigma_{Lcu} < \sigma_1 < \sigma_{Ltu} \\ -\sigma_{Tcu} < \sigma_2 < \sigma_{Ttu} \\ |\tau_{12}| < \tau_u \end{cases}$$

Maximum strain theory In the case of the maximum strain theory, the failure of the lamina is predicted when one of the five local strains exceed one of the fracture strain.
For the Maximum strain theory the five main strain parameters are:

- Longitudinal tensile strain ε_{Ltu}
- Transversal tensile strain ε_{Ttu}
- Longitudinal compressive strain σ_{Lcu}

- Tensile compressive strain σ_{Tcu}
- In-plane shear strain τ_u

For this theory, the inequality that have to be respected not to have a failure in the lamina are the following. Also in this theory it is enough that one of the inequality is not respected and the failure occur.

$$\begin{cases} -\varepsilon_{Lcu} = -\frac{\sigma_{Lcu}}{E_1} < \varepsilon_1 < \frac{\sigma_{Ltu}}{E_1} = \varepsilon_{Ltu} \\ -\varepsilon_{Tcu} = -\frac{\sigma_{Tcu}}{E_2} < \varepsilon_1 < \frac{\sigma_{Ttu}}{E_2} = \varepsilon_{Ttu} \\ |\gamma_{12}| < \gamma_u = \frac{\tau_u}{G_{12}} \end{cases}$$

Tsai-Hill failure theory Tsai-Hill failure theory is based on the deviatoric energy density failure theory, purposed by Von-Mises for isotropic materials[5]. Tsai criterion based on the distortion energy theory retain the material failed when the following inequality is not respected:

$$\begin{aligned}(G_2+G_3)\sigma_1^2 + (G_1+G_3)\sigma_2^2 + (G_1+G_2)\sigma_3^2 - 2G_3\sigma_1\sigma_2 - \\ +2G_2\sigma_1\sigma_3 - 2G_1\sigma_2\sigma_3 + 2G_4\tau_{23}^2 + 2G_5\tau_{13}^2 + 2G_6\tau_{12}^2 \geq 1\end{aligned}$$

In case of a plane stress that impose $\sigma_3 = \tau_{23} = \tau_{13} = 0$, the expression reduces to:

$$(G_2+G_3)\sigma_1^2 + (G_1+G_3)\sigma_2^2 - 2G_3\sigma_1\sigma_2 + 2G_6\tau_{12}^2 \geq 1$$

G constants of this theory can be evaluated by imposing that the equation is equal to one when $\sigma_1 = \sigma_{Ltu}; \sigma_2 = \sigma_{Ttu}; \sigma_3 = \sigma_{Ttu}; \tau_{12} = \tau_u$. The system of equation that has to be solved to obtain G values is

$$\begin{cases} (G_2+G_3)\sigma_{Ltu}^2 = 1 \\ (G_1+G_3)\sigma_{Ttu}^2 = 1 \\ (G_1+G_2)\sigma_{Ttu}^2 = 1 \\ 2G_6\tau_u^2 = 1 \end{cases}$$

Chang/Chang criterion is a linear criterion that divide the failure comparison between four failure modes, which are the tensile fiber failure, compressive fiber failure, tensile fiber failure and the compressive matrix mode. The equation that rule this criterion are:

$$\begin{cases} e_f^2 = \left(\frac{\sigma_{aa}}{X_t}\right)^2 + \beta\left(\frac{\sigma_{ab}}{S_c}\right)^2 - 1 \leq 0 \\ e_c^2 = \left(\frac{\sigma_{aa}}{X_c}\right)^2 - 1 \leq 0 \\ e_m^2 = \left(\frac{\sigma_{bb}}{Y_t}\right)^2 + \left(\frac{\sigma_{ab}}{S_c}\right)^2 - 1 \leq 0 \\ e_d^2 = \left(\frac{\sigma_{bb}}{2S_c}\right)^2 + \left[\left(\frac{Y_c}{2S_c}\right)^2 - 1\right]\frac{\sigma_{bb}}{Y_c} + \left(\frac{\sigma_{ab}}{S_c}\right)^2 - 1 \leq 0 \end{cases}$$

The idea of this failure criterion is that if one of the four inequalities becomes equal to 0, the element is considered failed. This mean that we are considering that for each element the failure can be caused by one of the four failure modes. This underline how it is important that both the matrix and the matrix have good mechanical properties and also that it is important to design the composite component to have a failure caused by the inequality that is describing the behavior of the most performing part of the composite.

1.5 Hybridization of composites materials

Composite materials are produced with technology that are relatively new and have many topic to be further investigated. Natural fibers composite is a technology that is even younger than composites materials and in the literature it is possible to find few technical paper about those, but the mechanical properties are usually not comparable with Glass or Carbon fibers. For this reasons the new studies are focus on studying the behavior of hybrid composite, manufactured by mixing natural fibers with conventional fibers. Most investigated hybridization usually combine Glass or Carbon fibers with Flax, Hemp or Basalt fibers.

The most interesting studies found in literature about hybrid composites are hereafter reported and briefly described

Investigation into the fatigue properties of flax fibre epoxy composites and hybrid composites based on flax and glass fibres [6]

The main focus of the article is an investigation and comparison of the mechanical properties of three laminates, Glass only fiber composite, Flax only composite and an hybrid composite with Flax and Glass fibers. These composites have been manufacturing using an autoclave and Prepreg fabrics, with a curing cycle at 3.5 bar with two ramps, from room temperature to 90°C with a ramp of 3°C/min and from 90°C to 120°C with a ramp of 2°C/min and ending the cycle with 60 minutes at 120°C and 3.5 bar. Firstly a mechanical characterization of the materials studied have been done, to find mechanical properties of the laminate such as Young moduli (E_1 and E_2), Poisson ratios ($\nu_{12}; \nu_{13}; \nu_{23}$, Shear moduli ($G_{12} = G_{13} = G_{23}$) and fracture energy ($G_{IC}$) that for sake of completenes are reported in table 1.2.

Table 1.2: Material Properties for Flax and Glass Laminates of article [6]

Material property	**Flax laminate**	**Statistical values**	**Glass laminate**
Longitudinal modulus, E_1 (GPa)	36.025	SDV = 3.941 CV = 10.94%	15.75
Transverse modulus, E_2 (GPa)	4.727	SDV = 0.142 CV = 3.012%	2.735
Poisson's ratio, ν_{12}	0.4487	SDV = 0.142	0.3
Poisson's ratio, ν_{13}	0.4487	CV = 31.56%	0.21
Poisson's ratio, ν_{23}	0.32		0.21
Shear modulus, $G_{12} = G_{23} = G_{13}$ (GPa)	2.8514	SDV = 2.836 CV = 0.781%	2.36
Fracture energy, G_{Ic} (N/mm)	1.3431	SDV = 0.241 CV = 17.9%	3.992

As it is also possible to understand looking at table 1.2, in the study unidirectional fabrics have been used. After investigating mechanical properties, using ASTM standards, fatigue tests have been performed, using also for this test standardized methods by ASTM. The stress levels applied to the specimens are between 0.45 and 0.7 times the ultimate tensile strength evaluated by the first tests. The results reported in table 1.3 indicates that the hybridization of composites increase the performances of the composite, increasing the average number of cycles that the specimen bore before breaking.

Table 1.3: Experimental results of fatigue tests of the article [6]

	0.7 UTS		0.6 UTS		0.5 UTS		0.45 UTS	
	N_{avg}	$\log(N_{\text{avg}})$	N_{avg}	$\log(N_{\text{avg}})$	N_{avg}	$\log(N_{\text{avg}})$	N_{avg}	$\log(N_{\text{avg}})$
Lam-F	18,278	4.26	12,048	4.08	520,374	5.71	567,038	5.75
Lam-C	34,662	4.54	115,999	5.06	269,223	5.43	1,200,000	6.11
Lam-D	69,214	4.84	194,499	5.29	226,416	5.35	695,309	5.84

Further investigation of specimen have been done using DMA tests and μ - CT scanning the fractured specimen from fatigue tests. Form DMA, the hybrid composites showed an higher storage modulus at high temperature, with a greater performance between 70°C and 140°C. From CT scanning, the behavior of flax do not change between Flax only and hybrid composite, but the fracture surface of the glass fibers are smoother. This article report that the hybridization of composite improve the performances of both single fiber type material, but also report that the delamination between flax and glass need to be investigated.

Improving the impact performance of natural fiber reinforced laminate through hybridization and layup design [7]

In this article a thick plate made out of many layers of an hybrid composite made out of glass and flax have been investigated. The layer orientation of the plies are 0, 90 and ±45 degrees.

The material used are unidirectional prepregs fabrics with the material properties reported in table 1.4.

Table 1.4: Material properties of FLAXPREG-T-UD-110 flax-epoxy and G10000/6510 glassfibre-epoxy [7]

Property	**Value**	**Remark**
NFRP		
Modulus (fibre direction)	35.0 GPa	ASTM D3039
Modulus (transverse direction)	2.2 GPa	ASTM D3039
Tensile strength (fibre direction)	365 MPa	ASTM D3039
Tensile strength (transverse direction)	3.87 MPa	ASTM D3039
Compressive strength (fibre direction)	136.9 MPa	[8]
GFRP		
Modulus (fibre direction)	61.6 GPa	ASTM D3039
Modulus (transverse direction)	11.8 GPa	ASTM D3039
Tensile strength (fibre direction)	1146 MPa	ASTM D3039
Tensile strength (transverse direction)	38.5 MPa	ASTM D3039
Compressive strength (fibre direction)	597 MPa	ASTM D6641

The stack up sequences studied in this article are represented in figure 1.4, where the numbers report the fibers orientation, the thickness of the ply is represented by the thickness of the cube representing that ply.

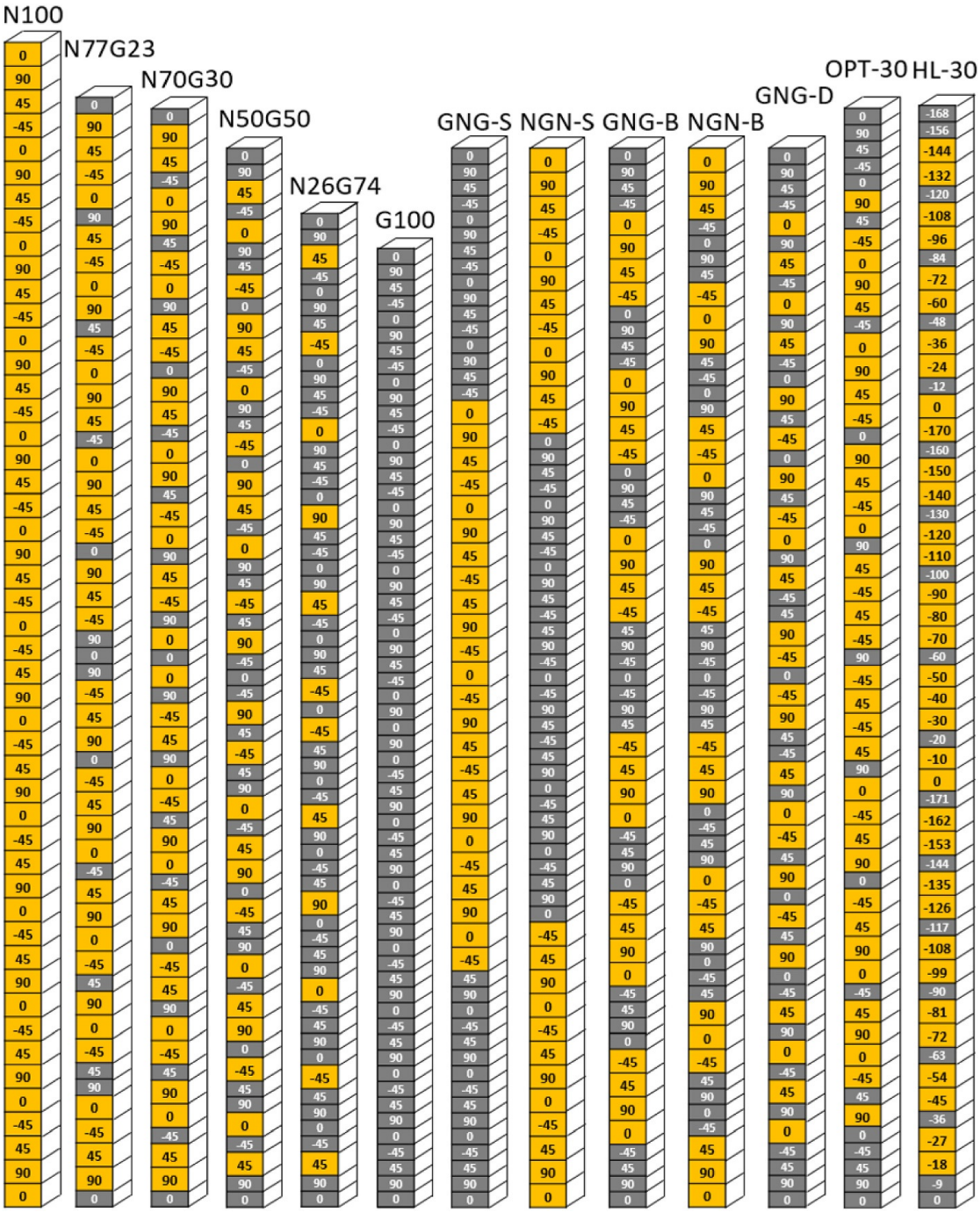

Figure 1.4: Layup configurations of tested laminates [7]

The impact have been performed with an adjustable mass with an interval of energy derivable to the plate that can be selected with 1J accuracy. The impact

have been performed always at 3.1 m/s.

The article report an improvement in the energy absorption of hybrid materials, with an overcome in performance of energy absorption of the hybrid composite made with only 30 wt% of glass fiber reinforcements. It is important to underline that the best performances have been obtained by placing as outer plies the sequence of glass plies.

Mechanical Characterization of Glass-Basalt Hybrid Composites with Different Fiber Weight Fraction [9]

This article investigate about mechanical properties of an hybrid composite made of Basalt and Glass fibers. Despite the other articles here reported, in this article the fabrics used in the composite material are plain fabrics and the composite have been obtained using the hand layup technique. The plates investigated in this study are reported in table 1.5, in total 5 plates have been manufactured.

Table 1.5: Laminate Stacking Sequence

Designation of Laminate	Stacking Order	Laminate Thickness (mm)
Laminate-A	G\G\G\G\G\G\G	3.07
Laminate-B	B\G\G\G\G\G\B	2.95
Laminate-C	B\G\B\G\B\G\B	2.86
Laminate-D	B\B\B\G\B\B\B	2.79
Laminate-E	B\B\B\B\B\B\B	2.75

An interesting result obtained in this paper is that the hybridized specimens results in having better mechanical properties than the Glass only or Basalt only. *"With glass-basalt hybridization, tensile strength was increased by 20%, flexural strength was increased by 12%, and impact strength was increased by 14% compared to only glass fiber laminate"*[9] Results are reported as Specific tensile strength, Specific flexural strength and Specific impact strength, the boxplots with the results are reported in figure 1.5

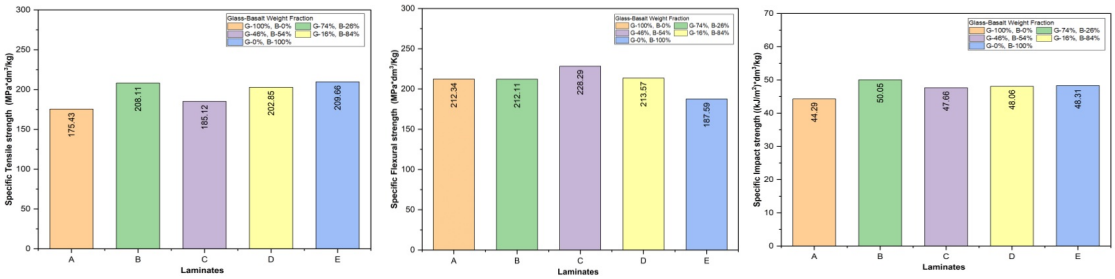

Figure 1.5: Specific Strength of different laminates [9]

Hybrid Flax/Glass composite

The objective of this thesis is the evaluation of mechanical properties of an hybrid E-Glass/Flax fabrics composite manufactured with bio-based resin with a percentage in plies of 50%-50% of the two different fabrics laminated together and the evaluation of a possible application in a crash absorber for a formula SAE car. An experimental campaign is necessary to evaluate the mechanical properties of the two composites to evaluate how well the two materials behave each other and if there is a favorite stack up sequence. After the experimental campaign, a numerical reproduction of the tests to set up suitable material cards that describes the behavior of the single laminae but that also reproduce all the four stack-up should be develop, thanks to this material cards the feasibility of the production of the crash absorber should be evaluated, considering the increment in weight if compared with a CF version of the same geometry.

Chapter 2

Experimental Methods and Procedures

2.1 ASTM standards

ASTM international, previously called American Society for Testing and Materials, is an international organization, based in the U.S. which publish technical standards used to test a wide range of materials. Thanks to standards it is possible to have results from test that can be comparable each other, increasing repeatability of each test. Standard that can be used for testing composite material are the one used in testing unenforced and reinforced rigid plastics, used both in testing particulate reinforced composites and fiber reinforced composites, both short fiber reinforced and long fiber reinforced.

2.1.1 Standards and Procedures Adopted

For the characterization of this materials, the mechanical properties evaluated are the following:

Table 2.1: Properties and corresponding standards used.

Properties	Standard used
E_1	D3039-D395
$E_2 = E_1$	D3039-D395
ν	D3039
$\sigma_{UTS,t}$	D3039
$\varepsilon_{max,t}$	D3039
$\sigma_{UTS,c}$	D395
$\varepsilon_{max,c}$	D395
E_f	D790
G	D5379
τ_{max}	D5379
γ_{max}	D5379

ASTM Standard D3039

This standard from ASTM is the one used for the tensile test specimen. It can be used to characterize Tensile Properties of Polymer Matrix Composite Materials. The summary that ASTM use to describe this test method is: *"A thin flat strip of material having a constant rectangular cross section is mounted in the grips of a mechanical testing machine and monotonically loaded in tension while recording the force. The ultimate strength of the material can be determined from the maximum force carried before failure. If the coupon strain is monitored with strain or displacement transducers then the stress-strain response of the material can be determined, from which the ultimate tensile strain, tensile modulus of elasticity, Poisson's ratio, and transition strain can be derived".[10].* The specimen used have a length of 250 mm and a transverse dimension of 25.4 mm The thickness of each specimen varies with the thickness of the plate from which it has been cut using a water-jet machine. The fixture used are the universal ones of the Instron machine. The strain Gage for each specimen have been applied to evaluate also the Poisson modulus. For each specimen, glass fiber tabs have been applied in the gripping length. For each specimen have been evaluated stress, strain, Young modulus, Poisson ratio and also the force and the displacement of the crossbar of the UTM.

ASTM Standard D790

This is the standard from ASTM which is used to evaluate bending properties of our composites. The summary that ASTM use to describe this test method is: *"A test specimen of rectangular cross section rests on two supports in a flat-wise position and is loaded by means of a loading nose located midway between the*

supports. Unless testing certain laminated materials (see 7 for guidance), a support span-to-depth (of specimen) ratio 16:1 shall be used. The specimen is deflected until rupture occurs in the outer surface of the test specimen or until a maximum strain of 5.0 % is reached, whichever occurs first".
Procedure A is designed principally for materials that break at comparatively small deflections and it shall be used for measurement of bending properties, particularly bending modulus, unless the material specification states otherwise. Procedure A employs a strain rate of 0.01 mm/mm/min (0.01 in./in./min) and is the preferred procedure for this test method.
Procedure B is designed principally for those materials that do not break or yield in the outer surface of the test specimen within the 5.0 % strain limit when Procedure A conditions are used. Procedure B employs a strain rate of 0.10 mm/mm/min (0.10 in./in./min).[11] To avoid buckling, with flax specimen it has been necessary to reduce the gauge length.

ASTM Standard D695

For compression behavior, Standard D695 have been used. *"This test method covers the determination of the mechanical properties of unenforced and reinforced rigid plastics, including high-modulus composites, when loaded in compression at relatively low uniform rates of straining or loading. Test specimens of standard shape are employed. This procedure is applicable for a composite modulus up to and including 41,370 MPa (6,000,000 psi)."[12]* It has been used a smaller universal testing machine, with a smaller and more accurate load cell.

ASTM Standard D5379

To compute Shear properties a v-notched specimen have been used following standard D5379. The summary present in the standard resume the test method as follow. *"A material coupon in the form of a rectangular flat strip with symmetrical centrally located v-notches, shown schematically in Fig. 2.4, is loaded in a mechanical testing machine by a special fixture (shown schematically in Fig. 2.2 and in more detail in the machining drawings of ASTM Adjunct. The specimen is inserted into the fixture with the notch located along the line of action of loading by means of an alignment tool that references the fixture. The two halves of the fixture are compressed by a testing machine while monitoring force. The relative displacement between the two fixture halves loads the notched specimen. By placing two strain Gage elements, oriented at 645° to the loading axis, in the middle of the specimen (away from the notches) and along the loading axis, the shear response of the material can be measured. The loading can be idealized as asymmetric bending, as shown by the shear and bending moment diagrams of Fig. 2.3 The notches influence the shear strain along the loading direction, making the distribution more*

uniform than would be seen without the notches. While the degree of uniformity is a function of material orthotropy, the best overall results, when testing in the 1-2 plane, have been obtained on [0/90]ns-type laminates."[13]

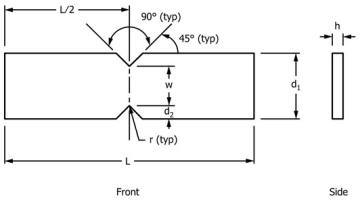

Figure 2.1: Geometry of the specimen

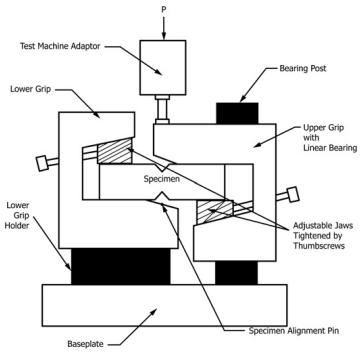

Figure 2.2: Fixture scheme

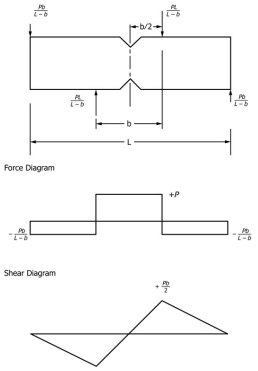

Figure 2.3: Loading diagrams

Figure 2.4: Figures from ASTM Standard D5379/D5379M[13]

For this test a DIC technology have been used, instead of consuming two extensometers for each specimen, that are necessary to evaluate the shear strain.

2.2 Universal testing machine

The universal testing machine from Instron, figure 2.5, has been the main equipment used to evaluate the mechanical properties of the laminates studied. This UTM is an hydraulic model and it is equipped with a 100 kN load cell. This testing machine is equipped with an encoder that control the displacement of the cross-head, that is moved using the servo-hydraulic system of the machine. In fact a huge pump that serve the entire laboratory is installed in a different room, which is climate controlled. This machine is computer controlled and it is possible to control the test parameters, such as the feed rate of the cross-head, and also the gripper pressure used to hold in position the specimen tested. This is useful to avoid, o at least limit the multi-axial stress state in the grasping area.

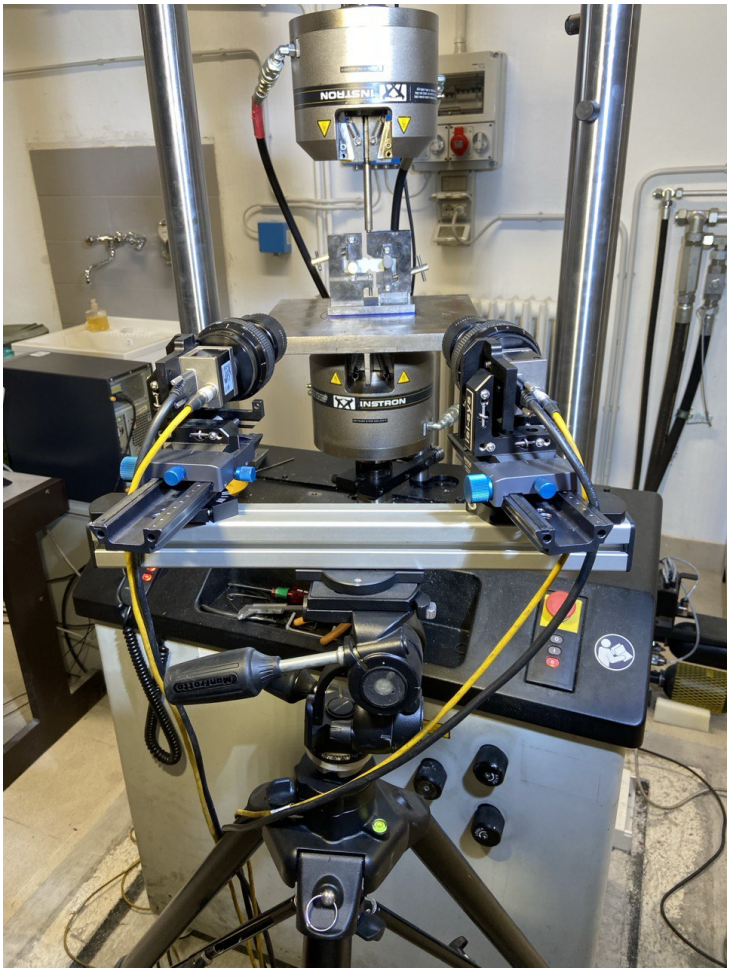

Figure 2.5: Instron universal testing machine during a Iosipescu shear strength test

Only for the bending properties tests a smaller universal testing machine,figure 2.6, with a 10 kN load cell and electro-mechanically controlled has been used, due to the small load that is necessary to applied at specimen during the test.

Figure 2.6: Universal testing machine used for bending tests

2.3 Strain Gage

A stain Gage is a sensor that use the property of a electric conductor material which resistance varies while deformed. If the sensor is mounted correctly, which means

that the portion of material at which is well bonded on is representative of hour material it is possible to consider that the strain evaluated with the strain Gage is the strain that the specimen or the component is experiencing. The resistance variation follow the following law:

$$\frac{\Delta R}{R} = \frac{\Delta \rho}{\rho} + \frac{\Delta l}{l} - \frac{\Delta A}{A}$$

where:

- R is the resistance (Ω)
- ρ is the resistivity of the wire/material ($\Omega \cdot \mathrm{m}$)
- l is the length of the wire (m)
- A is the cross-sectional area of the wire (m^2)

It is possible to demonstrate the previous equation, starting from the definition of the resistance of a resistor with section A and length l, with resistivity ρ, which is $R = \frac{\rho l}{A}$

$$\Delta R = \frac{\partial R}{\partial \rho}\Delta\rho + \frac{\partial R}{\partial l}\Delta l + \frac{\partial R}{\partial A}\Delta A = \frac{l}{A}\Delta\rho + \frac{\rho}{A}\Delta l - \frac{\rho l}{A^2}\Delta A$$

Evaluating now $\frac{\Delta R}{R}$, we obtain

$$\frac{\Delta R}{R} = \frac{\frac{l}{A}\Delta\rho}{\frac{\rho l}{A}} + \frac{\frac{\rho}{A}\Delta l}{\frac{\rho l}{A}} - \frac{\frac{\rho l}{A^2}}{\frac{\rho l}{A}}\Delta A = \frac{\Delta R}{R} = \frac{\Delta \rho}{\rho} + \frac{\Delta l}{l} - \frac{\Delta A}{A}$$

Considering now the value of ΔA in case of a rectangular area of dimensions $A = a \cdot b$

$$\Delta A = \frac{\partial A}{\partial a}\Delta a + \frac{\partial A}{\partial b}\Delta b = b\Delta a + a\Delta b$$

$$\frac{\Delta A}{A} = \frac{b\Delta a + a\Delta b}{ab} = \frac{\Delta a}{a} + \frac{\Delta b}{b} = -\nu\frac{\Delta l}{l} - \nu\frac{\Delta l}{l} = -2\nu\varepsilon$$

Considering now the equation $\frac{\Delta R}{R}$ for a rectangular resistance, as the ones of the common strain Gages, we obtain:

$$\frac{\Delta R}{R} = \frac{\Delta \rho}{\rho} + \frac{\Delta l}{l} - \frac{\Delta A}{A} = \varepsilon(1 + 2\nu) + \frac{\Delta \rho}{\rho} \approx 1.6\varepsilon + \frac{\Delta \rho}{\rho}$$

because ν of material used for the strain Gage is known and a linear approximation of the variation of the resistivity with the deformation can be done. The relationship

between the applied deformation and the resistance variation is called Gage Factor, noted as K, usually the producers of the strain Gages provide this value.

$$\frac{\Delta R}{R} \approx 1.6\varepsilon + \frac{\Delta\rho}{\rho} \quad K = \frac{\Delta R/R}{\varepsilon} \approx 1.6 + \frac{\Delta\rho/\rho}{\varepsilon}$$

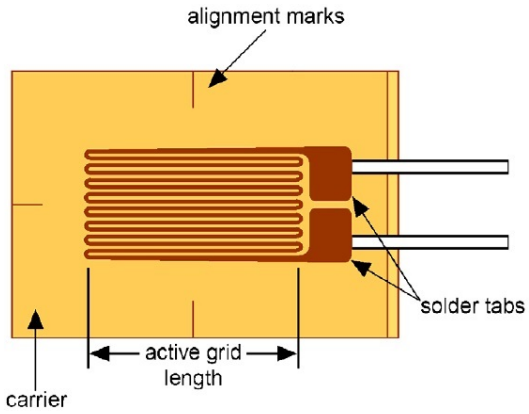

Figure 2.7: Strain Gage scheme [14]

The strain Gage positioning is made by bonding the strain Gage surface with the specimen surface, the adhesive used to bond the two surfaces is usually a cyanoacrylate or epoxy resins for longer tests. A clear scotch tape is used to take in position the strain Gage while the adhesive consolidate and it is helpful to align the strain Gage with the normal direction of the specimen. While testing metallic materials, the heat produced from the passage of current through the conductor is not a problem, it can be if the material tested is a polymer, for example while testing some plastics or composite materials, because the mechanical properties can be highly affected by the change of temperature. To avoid this problem the power supplied to the to the measuring instruments can be reduced. Another big issue related to the temperature related to those testing materials is the soldiering phase, where the electric cables are connected with the soldier tabs of the strain Gage. The soldering temperature of the tip is around 300 °C, which is an higher temperature then the curing temperature of a normal epoxy resin and higher then the melting temperature of many thermoplastics. Those materials can be locally altered and this can affect macroscopically their mechanical properties.

Voltage divider

After bonding the strain Gages it is necessary to acquire data of the strain Gages. To do that a Wheatstone bridge configuration is used. To understand the principles of the Wheatstone bridge, let's start by explaining how a voltage divider works.

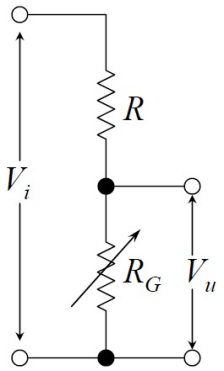

Figure 2.8: Voltage divider scheme [14]

The two V_i and V_u, indicated in pictures 2.8 can be chosen by imposing the two resistances.

$$V_u = \frac{R_G}{R + R_G} V_i \rightarrow V_u(R + R_G) = R_G V_i$$

If the R_G resistance varies and increase of a value ΔR_G, the two voltages varies as follow:

$$(V_u + \Delta V_u)(R + R_G + \Delta R_G) = (R_G + \Delta R_G)V_i \rightarrow$$

$$\rightarrow \Delta V_u = (V_i - V_u)\frac{\Delta R_G}{R + R_G} = V_i \frac{R}{R + R_G}\frac{\Delta R_G}{R + R_G}$$

This means that the variation of V_u is function of the variation of R_G This principle of functioning is used in a Wheatstone bridge.

Wheatstone bridge

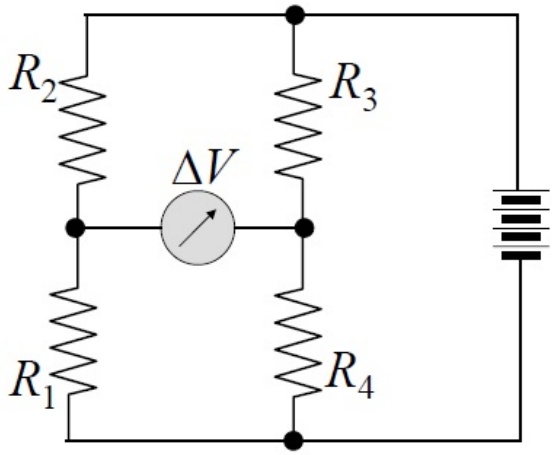

Figure 2.9: Wheatstone bridge scheme [14]

$$V_1 = \frac{R_1}{R_1 + R_2} V \quad V_4 = \frac{R_4}{R_3 + R_4} V$$

The difference in voltage noted on the picture as ΔV can be measured, and knowing that:

$$\Delta V = V_1 - V_4 = \left(\frac{R_1}{R_1 + R_2} - \frac{R_4}{R_3 + R_4} \right) V$$

Starting from a case where $\Delta V = 0$, an increment of R_1 can be evaluated measuring the voltage difference increment.

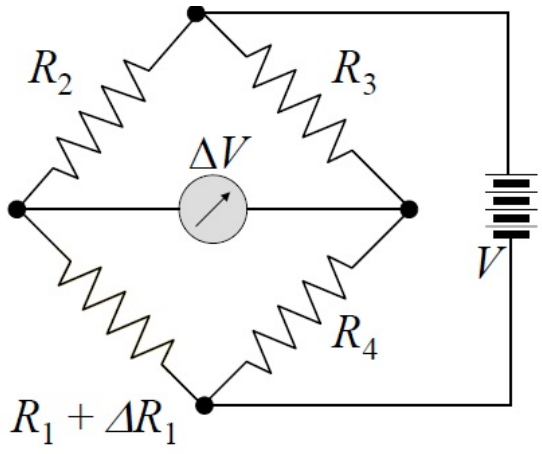

Figure 2.10: Wheatstone bridge scheme with R_1 as the strain Gage resistance [14]

If $R_1 = R_2$, the increment of R_1 can be evaluated as:

$$\Delta V \approx \frac{1}{4}\frac{\Delta R_1}{R_1}V \rightarrow \frac{\Delta V}{V} = \frac{1}{4}\frac{\Delta R_1}{R_1} = \frac{1}{4}K\varepsilon_1$$

Any resistance of the Wheatstone bridge can be composed by a strain Gage, for each resistance the strain evaluated, in case it is the only one resistance that is changing, will be:

- $\left(\frac{\Delta V}{V}\right)_{\Delta R_1} = \frac{1}{4}\frac{\Delta R_1}{R_1} = \frac{1}{4}K\varepsilon_1$
- $\left(\frac{\Delta V}{V}\right)_{\Delta R_2} = -\frac{1}{4}\frac{\Delta R_2}{R_2} = -\frac{1}{4}K\varepsilon_2$
- $\left(\frac{\Delta V}{V}\right)_{\Delta R_3} = \frac{1}{4}\frac{\Delta R_3}{R_3} = \frac{1}{4}K\varepsilon_3$
- $\left(\frac{\Delta V}{V}\right)_{\Delta R_4} = -\frac{1}{4}\frac{\Delta R_4}{R_4} = -\frac{1}{4}K\varepsilon_4$

$$\frac{\Delta V}{V} = \frac{K}{4}(\varepsilon_1 - \varepsilon_2 + \varepsilon_3 - \varepsilon_4) = \frac{K}{4}\varepsilon_{tot}$$

2.3.1 Strain Gage positioning

It is common to mount more than one strain Gage on a specimen, to measure other mechanical properties than the stress-strain curve. Here are reported some configurations and the way the strain Gages have to be mounted on the Wheatstone bridge scheme. The number reported in the yellow circles near the strain Gages in figures 2.12-2.19 indicate the resistance number of the Wheatstone bridge scheme reported in figure 2.11

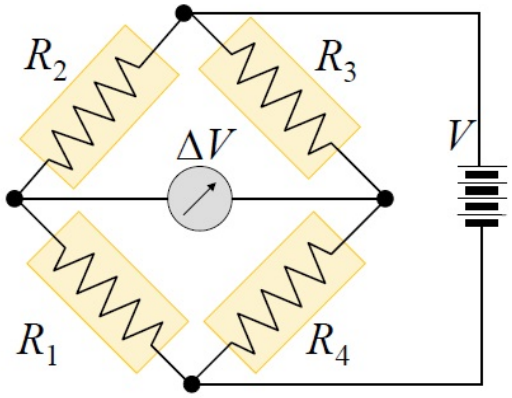

Figure 2.11: Wheatstone bridge scheme with resistances numbered [14]

Axial strain Gage only

In this configuration, only the axial deformation is evaluated.

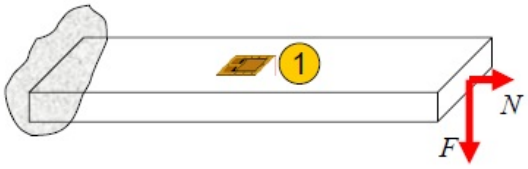

Figure 2.12: Strain Gage positioning [14]

This configuration has some issues, such as the fact that the apparent deformation is measured from the sensor and it is not possible to split the signal between the mechanical and the thermal deformation. Another inconvenience is related to the fact that if a bending behavior occur, as it can happen due to a buckling effect of the fibers in compression, it is not possible to notice it or distinguish between the deformation caused by the normal load application and the bending load application. If those issues are not relevant, this configuration is the easiest and cheaper to perform, and for this reason it is used. The deformation evaluated is:

$$\varepsilon_{tot} = \varepsilon_F + \varepsilon_N + \varepsilon_{\Delta T}$$

Axial strain Gage with temperature compensation

In this configuration, only the axial deformation is evaluated, but the thermal expansion contribution is compensated.

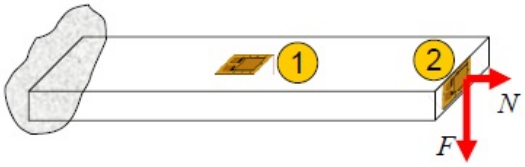

Figure 2.13: Strain Gage positioning [14]

With this configuration, the thermal expansion contribution is cleared away from the sensors output, but it is still not possible to distinguish between the strain caused by the normal load and the bending load. It is useful if the testing

conditions are not the one reported on the standards, but it is more costly because two strain Gages are required. The output obtained is:

$$\varepsilon_{tot} = \varepsilon_F + \varepsilon_N$$

Axial strain Gages for bending deformation evaluation

In this case, the two strain Gages are positioned in the opposite side of the specimen with the same direction. In case of pure normal stress, the two strain Gages theoretically measure the same deformation and the output will be zero.

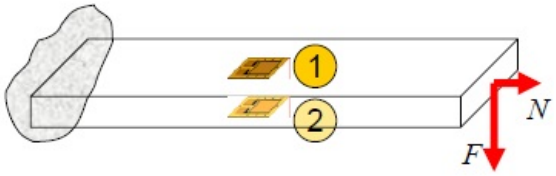

Figure 2.14: Strain Gage positioning [14]

The thermal effect and the normal deformation are deleted by compensating them between the two strain Gages. With this configuration, the bending deformation is amplified by a factor 2.

$$\varepsilon_{tot} = 2 \cdot \varepsilon_F$$

Axial strain Gages for normal deformation evaluation

Using the second axial strain Gage as the third resistance, instead the second, the bending deformation is compensated and the deformation measured is only axial.

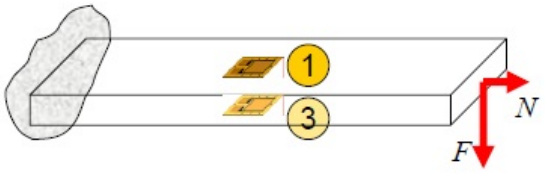

Figure 2.15: Strain Gage positioning [14]

With this configuration the thermal effect is not compensated and the total deformation evaluated are:

$$\varepsilon_{tot} = 2 \cdot \varepsilon_N + 2 \cdot \varepsilon_{\Delta T}$$

Axial and transverse strain Gage for normal and bending deformations with Poisson

Using two strain Gages positioned perpendicularly each other, it is possible to compensate thermal expansion and obtain a total deformation that also includes the Poisson ratio value.

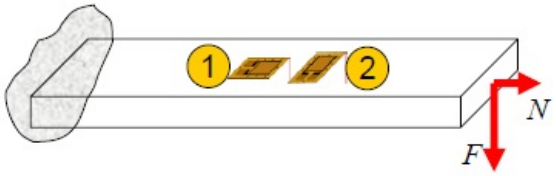

Figure 2.16: Strain Gage positioning [14]

Deformations due to normal and bending loads cannot be distinguished. The output value is:

$$\varepsilon_{tot} = (1 + \nu) \cdot \varepsilon_F + (1 - \nu)\varepsilon_N$$

Axial and transverse strain Gage for bending deformation and Poisson ratio

Using for strain Gages, one for each resistance of the Wheatstone bridge, it is possible to obtain the deformation due to bending load multiplied by a factor that is function of the Poisson ratio.

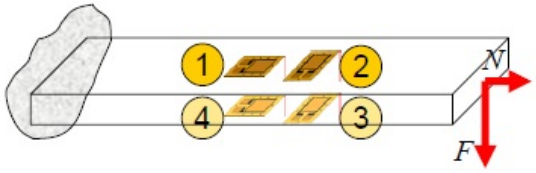

Figure 2.17: Strain Gage positioning [14]

Apparent deformation due to temperature and normal load deformation are compensated and mounting misalignment sensitivity is decreased. The only throwback is the fact that it is necessary to install four strain Gages.

Four axial strain Gages for pure bending deformation

If four strain Gages are mounted, all of them parallel to the normal direction of the specimen, the deformation due to bending load is measured.

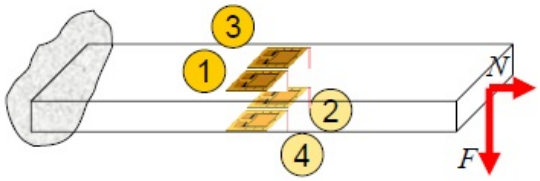

Figure 2.18: Strain Gage positioning [14]

Using four strain Gages, misalignment sensitivity is reduced and the bending deformation evaluated is more precise. The total deformation measured is equal to four times the bending deformation

$$\varepsilon_{tot} = 4 \cdot \varepsilon_F$$

Axial and transverse strain Gage for normal deformation only

Using four strain Gages is possible to isolate the deformation due to normal load, compensating the deformations due to the bending and the thermal loads.

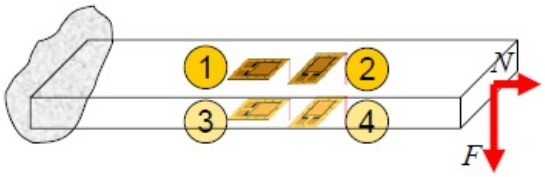

Figure 2.19: Strain Gage positioning

The only disadvantage of this configuration is correlated with the cost of the strain Gages, because it is compulsory to install four of them for each specimen. The signal obtained from the Wheatstone bridge is the deformation due to pure normal load multiplied for a factor $2(1 + \nu)$

$$\varepsilon_{tot} = 2 \cdot (1 + \nu) \cdot \varepsilon_N$$

Strain Gages have a throwback that is correlated to the fact that at a certain point the material of which the resistance is composed yields. This means that with this technology only the first part of the stress-strain curve can be computed. Usually the strain Gage yield after the last point used to compute the material properties following ASTM standards directives, for this reason they are widely used, especially when the number of specimen tested are not huge, because of the cost of this sensors that can be used for only one specimen and then they have to be replaced.

2.3.2 Knife-edge extensometer

This instrument is an alternative to strain Gages. This type of sensor can be used several times, because at hte end of the test it is not damaged by the test itself and can be mounted on the next specimen. It is also easier to be positioned on the specimen, having the knife edges that penetrate the surface of the specimen and, using springs or rubber bands, the extensometer is taken in position during all the test.

Figure 2.20: Knife-edge mono axial extensometer

During deformations, this instrument need to be taken off the specimen before the specimen breakage, for this reason it is necessary to stop the UTM movement for a while, to remove the extensometer. In some cases, some Universal Testing Machines are equipped with a steel bar that take in position the extensometer and not let it fall after the breakage of the specimen, it is useful to have a more accurate curve but the instrument needs to be calibrated more frequently.

Having an extensometer base that is bigger than the base of a strain Gage, this extensometer report a deformation that describe better the macroscopic behavior of the material, while using a strain Gage that have a smaller elongation basis, the measurements can be affected by local behavior. This can occur with composite materials with long fiber reinforcements, both for fabric and unidirectional materials. In case of fabrics, if the weaving threads are loosely woven, the dimension of the thread are bigger and in case of twill materials it is possible that the extensometer basis is fully bonded on warp only or weft only area. This means that the deformation that is measured for the extensometer is related to a microscopic behavior of the material. ASTM standards oblige the technician to bond the extensometer on an area that is Representative of the macroscopic material.

2.4 Digital Image Correlation (DIC)

This technology solve the problems of both sensors already analyzed. It is based on using a stereo-camera to measure the deformation of the specimen or of the part that we are analyzing. Using two cameras, it is possible to correlate the two images to evaluate also the depth of the video taken. The specimen need to be enlightened in the correct way to have the correct brightness of the images taken. The surface of the specimen have to be treated using paintings to have a bright background with very dark dots. The instrument requires a certain number of dot for each pixel, this mean that the surface has to be painted with a dense number of dots. Usually the specimen is white painted and the dots are made with a black spray painting.

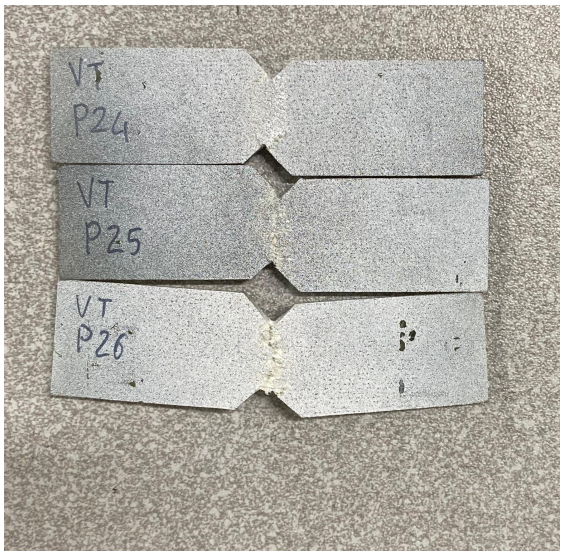

Figure 2.21: Iosipescu specimen painted for DIC

Every measurement have to be correlated with a calibration session, that can be done with a grid of points manually or automatically moved, positioned as closer as possible as the final position of the specimen.

Calibration can be performed before starting the measurements, between testing two specimens, or after testing each specimen. The crucial point is that the cameras must not be moved during the specimen testing or before being calibrated again after all the tests are completed.

Before starting each test, a software helps in positioning the lights to have as much as possible the surface of the specimen to have less noise possible during the measurements and to know in a bigger area possible the deformations, because the software evaluate the strain of the material for each pixel, after that it reports

the strain in a matrix with the value of each pixel included in the working area selected.

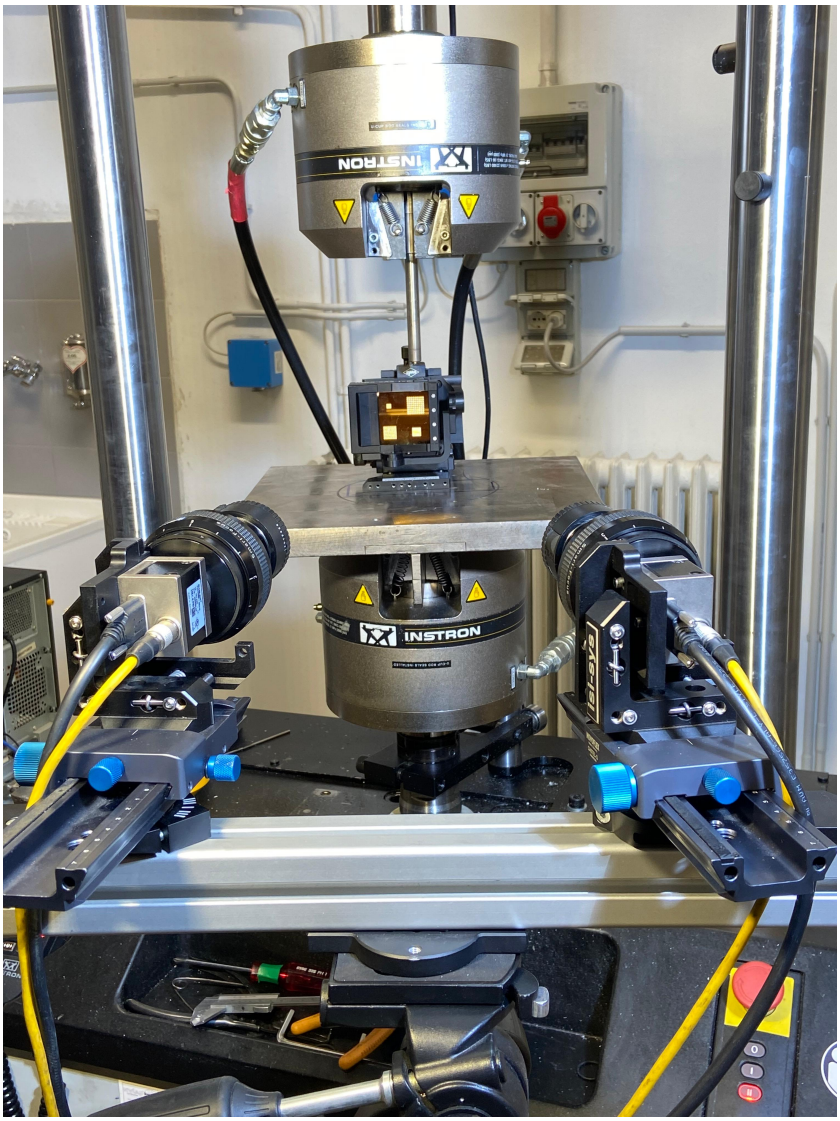

Figure 2.22: Calibration routine for the cameras

During the measurements images are collected and only afterwards data are elaborated. The area from where the points are evaluated has to be chosen form the first picture that DIC cameras collect, after that, thanks to the dots painted on the top, the program follow the area and report the results point by point in a matrix. The results can be shown also point by point plotting the area analyzed, like how it is reported in picture 2.23b. The area used for the specimen in this

study is reported in picture 2.23a.

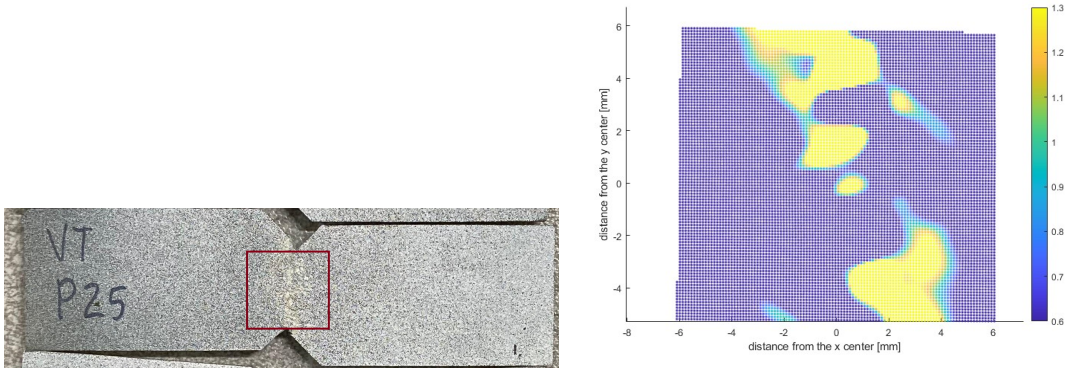

(a) Area analyzed for shear strain in the specimen **(b)** Strain reported point by point from DIC

Figure 2.23: Input and output of the DIC data elaboration

Chapter 3

Material characterization

During this work, four plates with different lamination sequences have been produced, with also other two plates with flax only or glass only reinforcements. All the four plates have a lamination sequence that is symmetric, to avoid internal stresses due to production processes. Each of the four hybrid plates have been produced with eight plies. Two of them have been produced by alternating the material of each layer, except from the two layer in the middle of the laminate, with the outer layers made of flax in one layer and glass in the other. The other two plates have been manufactured by alternating the material of the reinforcement every two layers. In figure 3.1, are reported the schemes of the lamination.

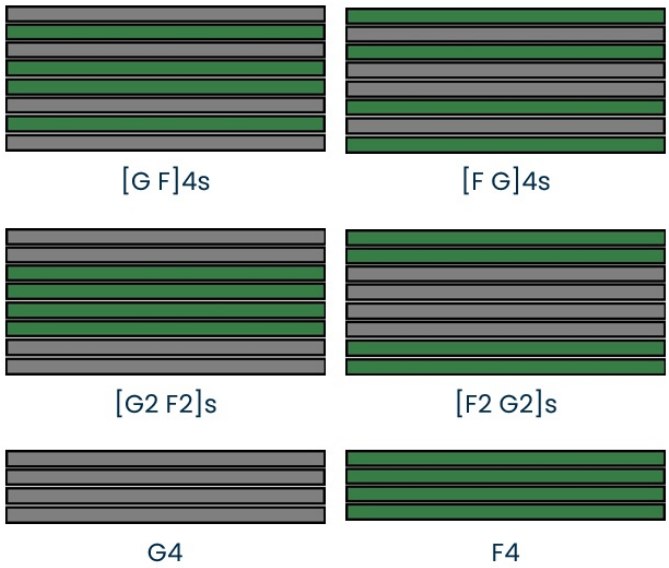

Figure 3.1: Stacking sequences of the tested materials

Other two plates made fully with flax fibers or glass fibers fabrics, each one with four plies, have been manufactured to evaluate the single lamina mechanical properties. The four plates have been manufactured using vacuum infusion technology, using a flat surface obtained with a glass plate. Wax have been used as release agent and the vacuum bag have been applied only on one side of the plate, using a sealant for vacuum bags as interface between the bag and the glass.

On the vacuum bag side a peel ply and a flow mesh have been used during lamination. With all the six plates the same peel ply and flow mesh have been used to avoid external factor that can cause some changes and having the same impregnation.

Bio-based epoxy resin have been mixed with the hardener and air have been taken of from the mix letting the resin in a vacuum environment for some minutes, until all the air bubbles do not appear anymore. After taking out all the air, the infusion process can be started, first of all the vacuum bag is depressurized as much as the vacuum pump can, than the resin is connected and, thank to the low pressure in the vacuum bag, it is sucked in and it impregnate all the fabrics. The curing cycle have been performed in an industrial oven for 8 hours at 80°C, as suggested in the resin TDS, that can be found in the official website of Easy Composites for the product IB2 Epoxy Infusion Bio Resin[1]. Even if the six plates have been manufactured with the same technique, the capability of getting impregnated and the trapped air within fabrics taken of is different and we can expect a small difference in the plates if we consider the volume content of resin and fibers in the composite.

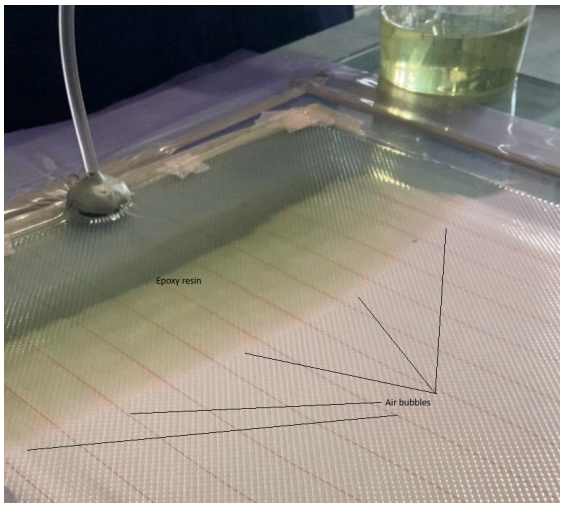

Figure 3.2: Resin infusion in the E-glass only material plate

[1]https://www.easycomposites.eu/IB2-epoxy-infusion-bio-resin

Internal voids are quite common when using this production technology, even if the resin is treated in a vacuum environment to remove as much trapped air possible, while sucking it into the bag, it is always possible to see bubbles of air that flow in the material, in figure 3.2 air bubbles in front of the resin flow are pretty evident, and the amount of voids that remains inside the material can be influenced from the stacking sequence. Fortunately, the impregnation and the curing cycle performed on the plates have been done properly and the laminates have a reduce amount of voids that are not visible with the naked eye. Figure 3.3 report the transversal cross section of one of the specimen tested where it is possible to see that no voids are visible.

Figure 3.3: Flax bending specimen

To evaluate the volume content of fibers and resin the equations 3.1-3.2 have been used. To be more understandable, in figure 3.4 it is reported a specimen where the reference system is reported.

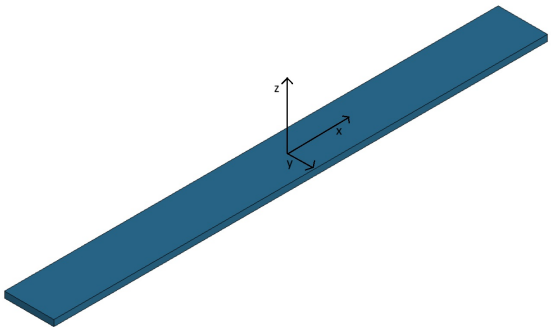

Figure 3.4: Reference system of the plates and of the specimen

$$\text{fiber volume} = \frac{\text{fabric areal weight}}{\rho_{material}} z_{section} \tag{3.1}$$

$$\text{matrix volume fraction} = 1 - \frac{\text{n° plies}_{\text{glass}}\text{fiber volume} + \text{n° plies}_{\text{flax}}\text{fiber volume}}{\text{specimen total volume}} \tag{3.2}$$

The volume fraction have been evaluated using the average thickness of all the specimen cut from each plate and they are reported in table 3.1

Table 3.1: Fibre and matrix volume fraction

Volume fraction	**[G F]4s**	**[F2 G2]s**	**[G2 F2]s**	**[F G]4s**	**Flax**	**Glass**
Fiber	34.01%	34.82%	33.88%	34.33%	33.92%	36.77%
Matrix	65.99%	65.18%	66.12%	65.67%	66.08%	63.23%

From table 3.1, it is possible to notice that glass fiber tend to trap less resin, but the difference in volume fraction is not that big if compared with the flax laminate volume fraction. This can slightly influence all the properties, favoring mechanical properties of the plate where four glass layer are laminated in sequence and the four layers of flax are laminated as outer layers.

3.1 Specimen preparation

All the specimen have been cut from the plates using a water jet machine, as suggested in the standards. Due to limited material availability, only one plate for each stacking sequence have been manufactured and for this reason the material have been characterized only along 0° direction. This lack of material also impose us only to test three specimen with ASTM standards D3039, D695 and D5379. All the specimens have been prepared following ASTM procedures and where needed, tabs have been applied in the surfaces that be in contact with the machine gripping fixtures. In this case only for tensile specimen tabs have been used. An epoxy resin have been used as bond agent between tabs surfaces and specimen surface. During this experimental campaign, glass fiber tabs have been used, due to luck of material, even if from standards it is required that tabs should be manufactured with a material with lower mechanical properties than the material tested.

3.2 Mechanical test

All the test have been performed in the laboratories of DIMEAS at Politecnico di Torino, between 16th and 20th of October 2023, except for Glass compression and shear, done the 25th of March 2024 and bending test the 10th of April 2024. Since the room where the UTM is positioned has a controlled environment, the test should not be affected from external aspects.

3.2.1 Tensile specimen

Following the standard guide lines, the tensile specimen have been cut with dimension of 250 mm x 25 mm, with the 250 mm dimension parallel to the zero direction of the laminate.

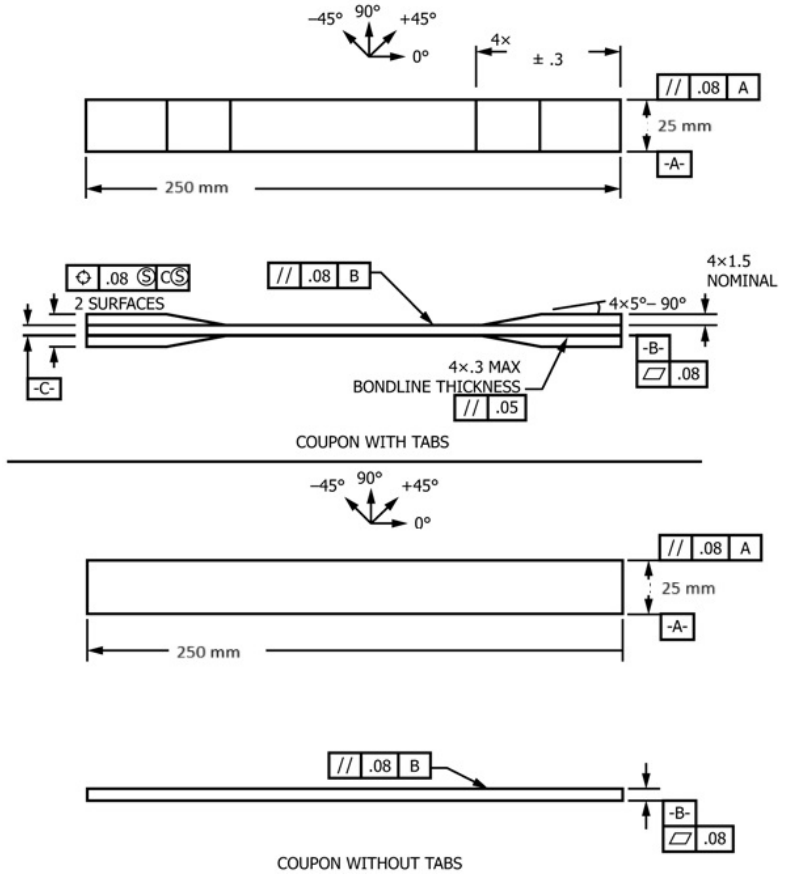

Figure 3.5: Specimen dimension [10]

Three specimen for each plate have been manufactured and two strain Gage to measure 0° and 90° deformation have been positioned on two out of three specimen, as it is possible to see from picture 3.6

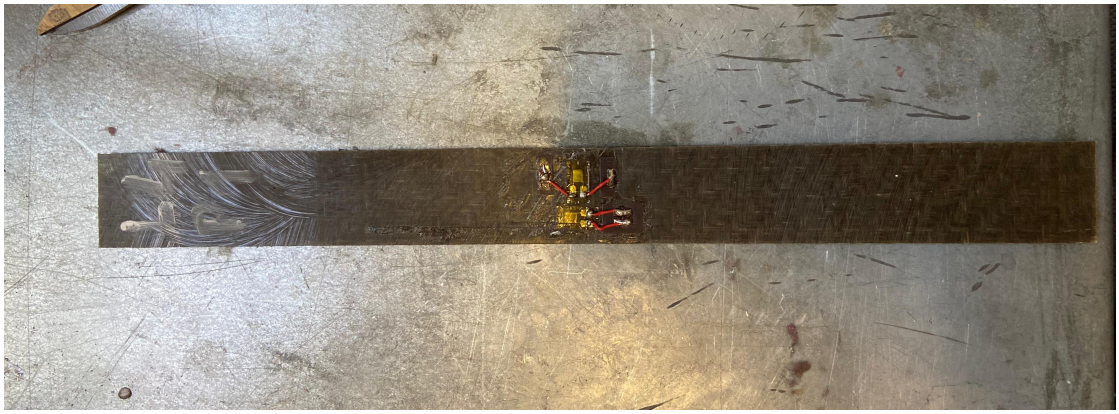

Figure 3.6: $[G_2F_2]_{2s}$ specimen one after the bonding of the strain Gage

After performing all the tests and elaborating all the data obtained, the results have been reported in table 3.2. With this configuration the material properties obtainable are the Young modulus, the Poisson ratio and the ultimate tensile strength.

Table 3.2: Tensile properties of the materials

	$[G\ F]_{4s}$	$[F_2G_2]_{2s}$	$[G_2F_2]_{2s}$	$[F\ G]_{4s}$	F_4	G_4
E [MPa]	13015 ± 799	13660 ± 820	13210 ± 933	13865 ± 2058	11155 ± 502	18525 ± 813
σ_{UTS} [MPa]	128 ± 11	153 ± 7	140 ± 1	143 ± 7	109 ± 17	224 ± 21
ν [-]	0.067 ± 0.026	0.068 ± 0.004	0.05 ± 0.018	0.05 ± 0.014	0.05 ± 0.016	0.067 ± 0.001

For the sake of completeness, in figure 3.7, the Young moduli are reported in a box plot with standard deviations.

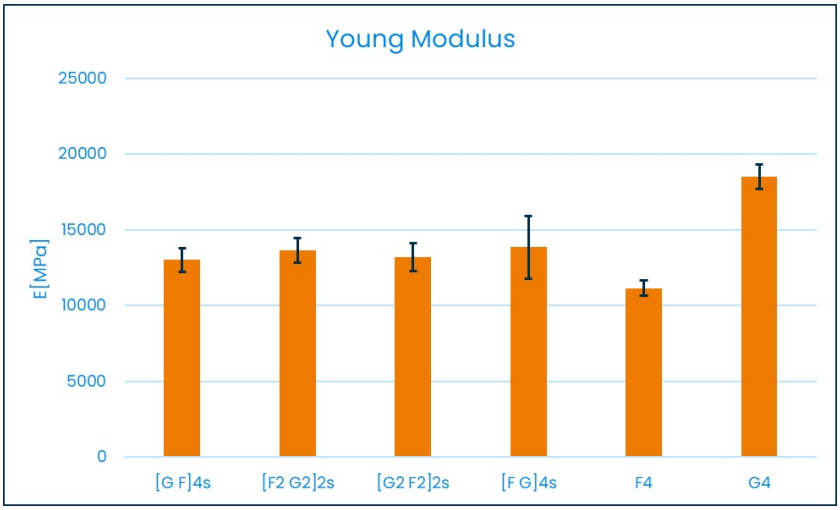

Figure 3.7: Graph of tensile Young's Moduli of Materials

3.2.2 Compression specimen

Compression specimen have been water-jet cut with dimensions 140 mm x 10 mm, with longer dimension parallel to 0°. After the first specimen tested, the 0° direction dimension have been decreased to avoid buckling, by cutting it with a diamond blade. In figure 3.8 it is reported the ASTM figure that report the geometries of the specimen.

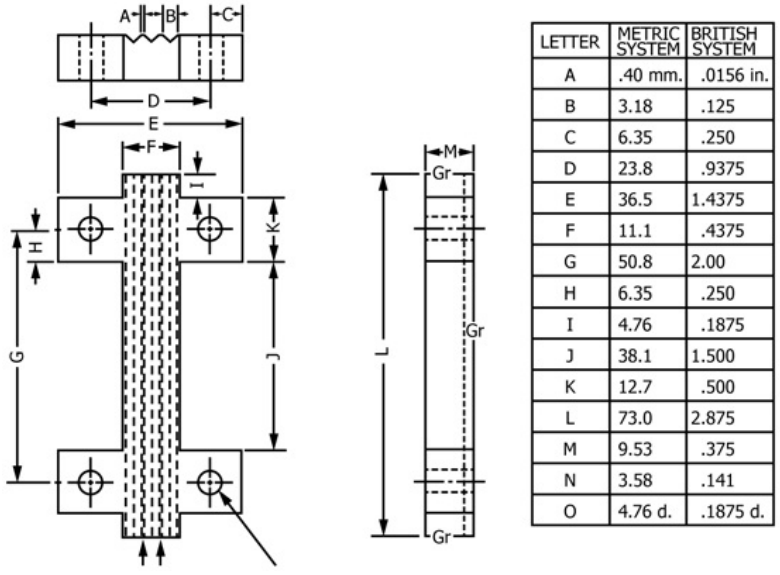

LETTER	METRIC SYSTEM	BRITISH SYSTEM
A	.40 mm.	.0156 in.
B	3.18	.125
C	6.35	.250
D	23.8	.9375
E	36.5	1.4375
F	11.1	.4375
G	50.8	2.00
H	6.35	.250
I	4.76	.1875
J	38.1	1.500
K	12.7	.500
L	73.0	2.875
M	9.53	.375
N	3.58	.141
O	4.76 d.	.1875 d.

Figure 3.8: Specimen dimension [12]

For compression specimen, only one strain Gage have been bonded in 0° direction. In this specimen it is relevant the position of the strain gauge not to be inside the anti buckling armor. In figure 3.9 it is possible to see all the specimen tested with the strain Gage already bonded. After performing all the tests and elaborating

Figure 3.9: Specimen tested following ASTM D695

all the data obtained, the results have been reported in table 3.3. With this configuration the material properties obtainable are the Young modulus and the ultimate compressive strength.

Table 3.3: Compressive properties of the materials.

	$[G\ F]_{4s}$	$[F_2G_2]_{2s}$	$[G_2F_2]_{2s}$	$[F\ G]_{4s}$	F_4
E [MPa]	12775 ± 290	12197 ± 4207	13270 ± 1207	11370 ± 806	9283 ± 2586
σ_{UCS} [MPa]	132 ± 9	135 ± 18	136 ± 16	143 ± 2	80 ± 4

As already done for tensile properties, the same box plot with compression results have been reported in figure 3.10

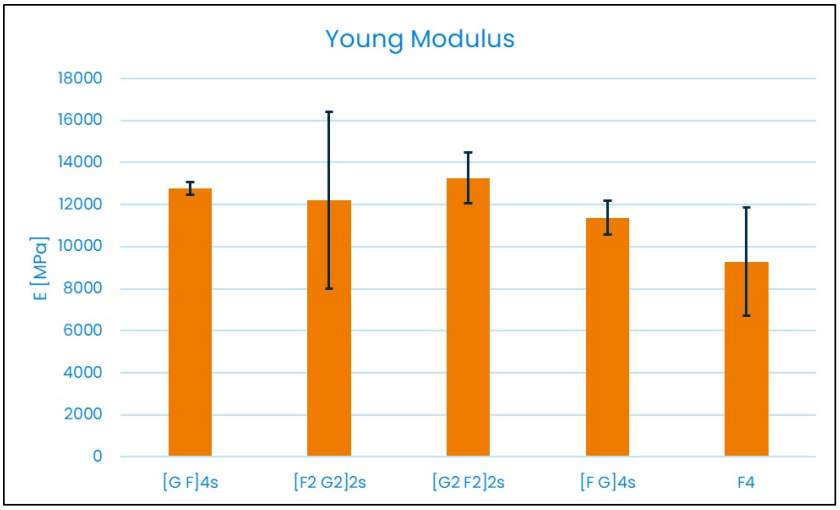

Figure 3.10: Graph of compressive Young's Moduli of Materials

3.2.3 Shear specimen

The shear properties have been obtained using a notched specimen. Standard ASTM D5379 use a fixture purposed by Iosipescu. The specimen geometries are the one reported in figure 3.11, where it is reported the figure purposed on the ASTM standard.

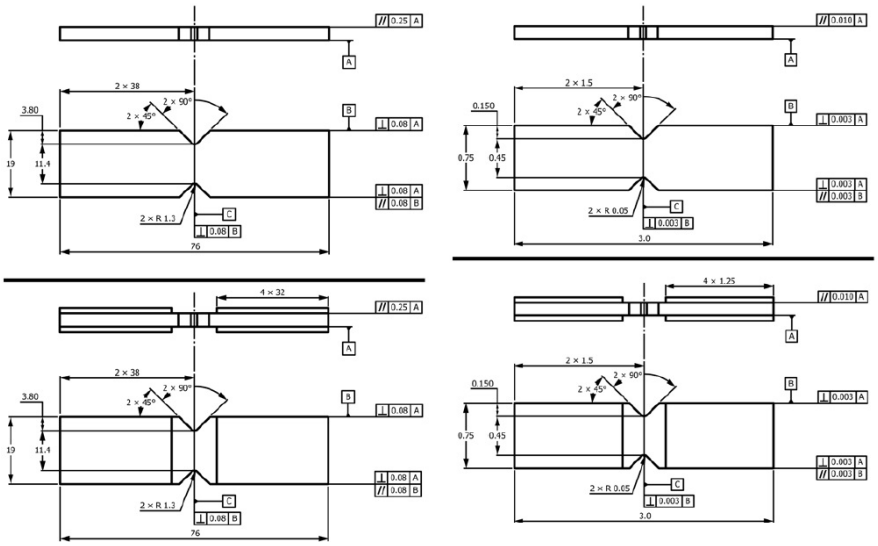

Figure 3.11: Specimen dimension [13]

Because of the needs of using two strain Gages to evaluate the shear properties,

DIC technology have been used to evaluate strain instead. DIC technology have been already explained in previous section. The surface have been painted as it is possible to see in figure 3.12, to be further processed by the computer.

Figure 3.12: Painted surface of a tested specimen

The results obtained from those specimen are reported in the table 3.4.

Table 3.4: Shear properties of the materials

	$[G\ F]_{4s}$	$[F_2G_2]_{2s}$	$[G_2F_2]_{2s}$	$[F\ G]_{4s}$	F_4	G_4
G [MPa]	2316 ± 13	2233 ± 75	2186 ± 11	2071 ± 42	1906 ± 59	3679 ± 483
σ_{UTS} [MPa]	53 ± 0.8	50 ± 1	51 ± 0.1	54 ± 0.6	46 ± 1.0	77 ± 1.0

Shear properties, as already done for the other mechanical properties, are reported in box plot 3.13

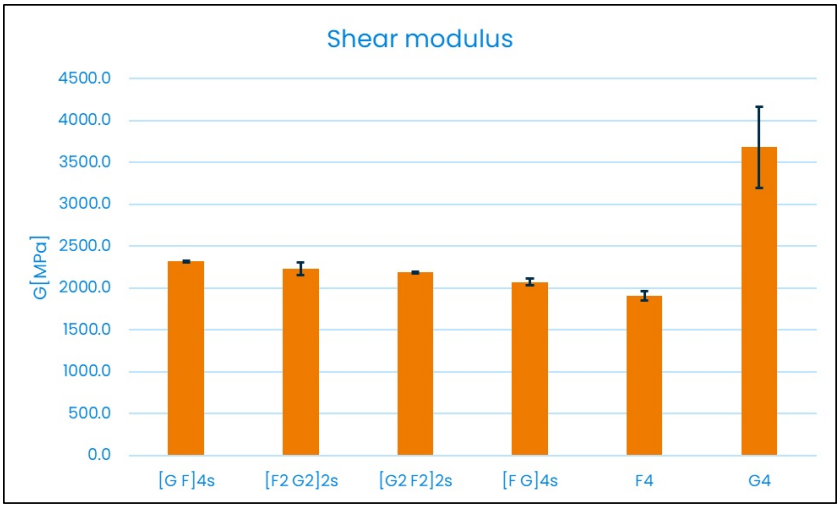

Figure 3.13: Graph of shear Moduli of Materials

3.2.4 Bending specimen

Finally the bending properties have been evaluated using ASTM Standard D790. No strain Gages have been used since it is not required from standards. The distance of the supports have to be chosen based on the average thickness of the specimen.

Figure 3.14: Two tested bending specimen

The results obtained are reported in table 3.5

Table 3.5: Bending properties of the materials

$E[Mpa]$	$[GF]_{4s}$	$[F_2G_2]_{2s}$	$[G_2F_2]_{2s}$	$[FG]_{4s}$	F_4	G_4
	10113±600	8138±545	11144±700	8981±600	3713±400	19832±282

Also for bending properties are reported in a box plot 3.15

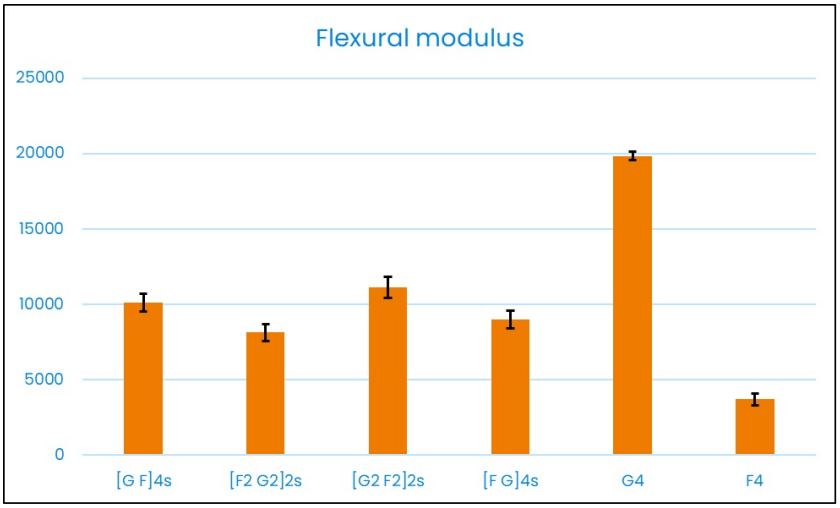

Figure 3.15: Graph of bending Moduli of materials

3.3 Results

For better comparing the mechanical properties of the plates, box plots that report all the properties together have been reported here after in 3.16 and 3.18. First of all the Young Moduli:

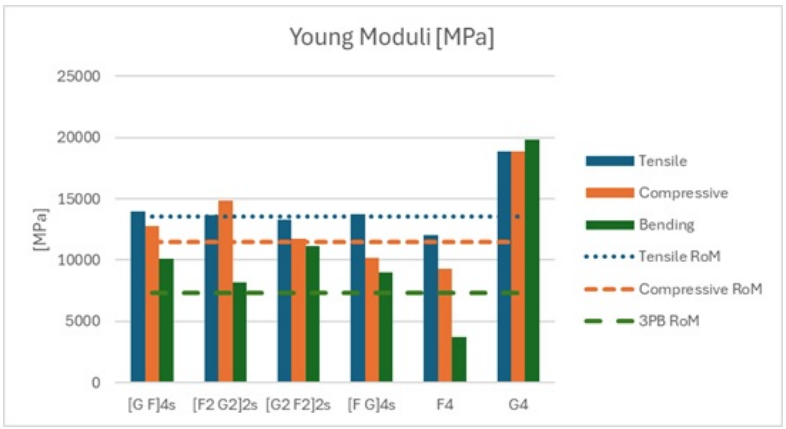

Figure 3.16: Comparison of the mechanical properties of the materials tested

For clarity, the shear modulus have been separated from the others, to have a reduced y scale and appreciate more how it changes between the different layups, in figure 3.17

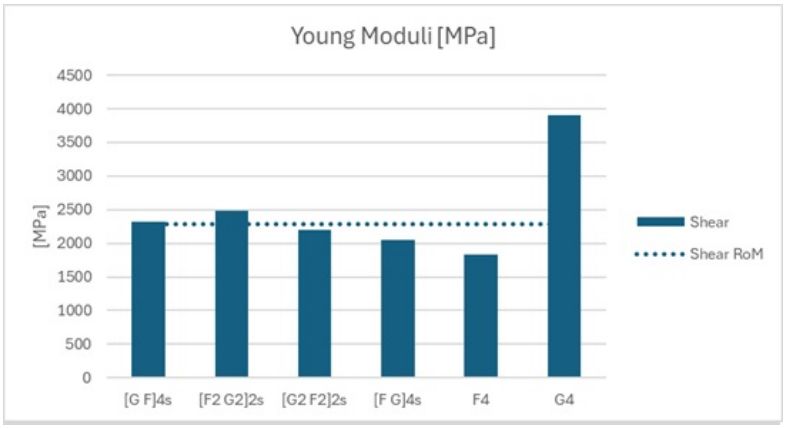

Figure 3.17: Comparison of the Shear modulus of the materials tested

It is possible to see that the only property that really change is the bending moduli, because it is influenced on the very last ply properties.

The other property compared is the ultimate tensile strength, where only the values at traction, compression and with Iosipescu test.

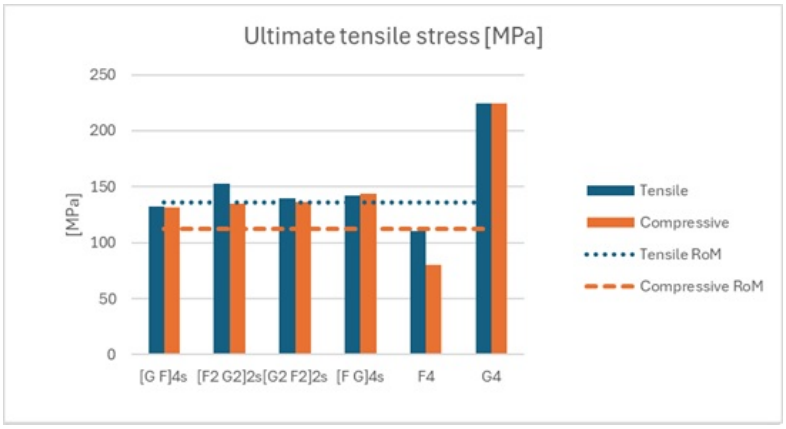

Figure 3.18: Comparison of the ultimate tensile strengths of the materials tested

Also the ultimate tensile strength is not really influenced by changing the lamination sequence, except for the second specimen, probably it's influenced because four consecutive layers are made of glass, that as it is possible to see, has an higher UTS than flax. Also for UTS, the shear UTS have been divided from the other stresses.

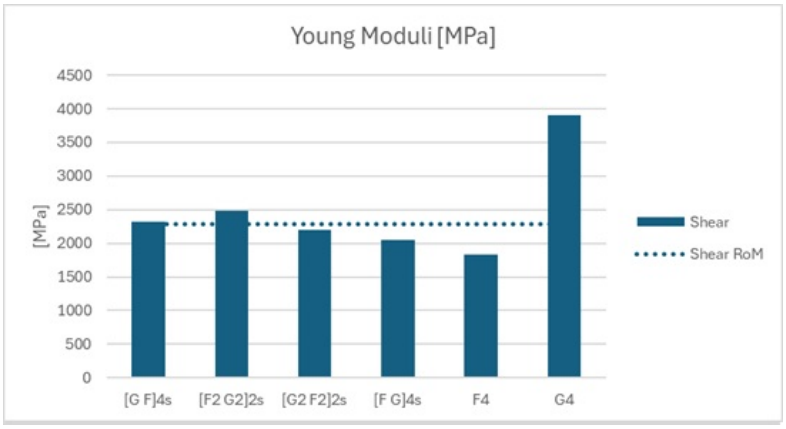

Figure 3.19: Comparison of the ultimate tensile strengths of the material tested at shear

Chapter 4

Finite element analysis

4.1 Introduction to finite elements analysis

In structural mechanics it is necessary to identify the physics reality. This process needs to be done connecting an experimental campaign with mathematics.

The flowchart[15] reported in figure 4.1 represent the flow of the process that has to be followed during this work. The numerical modeling can have some errors that can be connected to the simplifications used during the model creation or due to errors that can be done while writing the numerical model. For this reason it is necessary to validate the numerical model with experimental test, to use those parameters in any other model. During this thesis work, the numerical models are limited to structural problems and it has been validate using quasi-static test conditions as suggested in the ASTM standards.

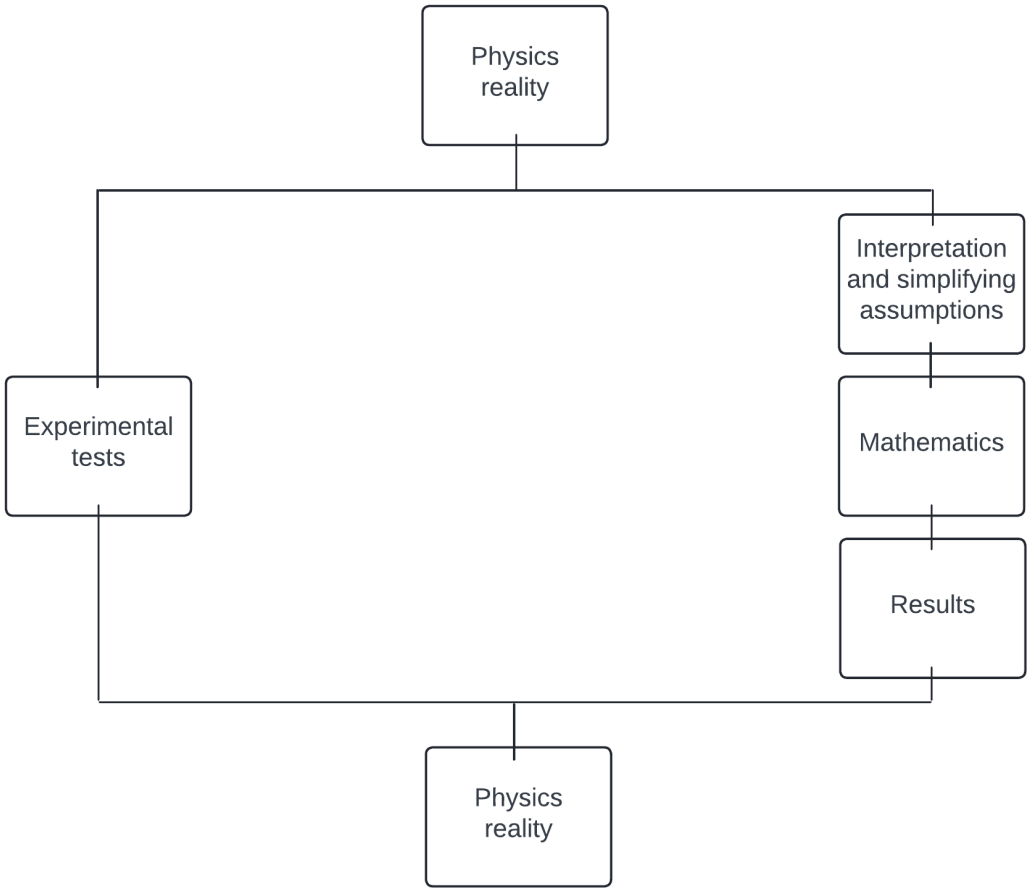

Figure 4.1: Parallel flow chart in structural mechanics

In finite elements method, the continuum domain is discretized using two entities, an element, that is the portion of the continuum, and the node, that is the point where two or more elements are connected. In figure 4.2 is reported a four node shell elements with the four nodes marked.

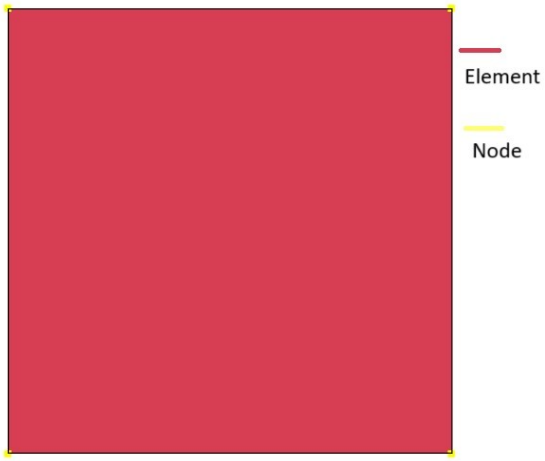

Figure 4.2: Four nodes shell element

4.2 Element type

In a FE analysis, it is possible to use a different type of elements, depending on the type of part that is going to be analyzed. Each type of element has a different amount of degrees of freedom. For each type of element it is also possible to have different integration and different number of nodes. Let's now report in table 4.1

Table 4.1: Type of elements in FE analysis

Element type	Number of nodes	DOF of each node
Truss element	2-3	1
Torsion element	2-3	1
Beam element 2D	2-3	3
Beam element 3D	2-3	6
Shell element	3-4-6-8	6
Solid element	3-8-10-20	3

4.2.1 Beam element

Is the simplest element used in FE analysis. It can be used to simulate lattice structures. It is used in many cases when the structure to be simulate tubular chassis or any other geometry that is easily depictable with beams or bars. Those elements can have two or three nodes, and depending on the number of those, the shape functions can be linear or quadratic.

4.2.2 Shell element

In case of a shell element it is possible to have three nodes elements, four nodes element or eight nodes element.
Three nodes elements have shape functions that are linear, this means that the deformation of the element is constant and so the stress of that.
Four nodes elements have a big range of applications. Shape functions are linear in both directions, this means that the stress inside the element is constant, but their stiffens is lower than a three nodes element, being in any case stiffer than the real material.
Eight nodes elements are the best element used for shell element analysis. Their shape functions are quadratic and this mean that the stress inside the element varies linearly along the border of the element. Three nodes element can be useful in some cases, for example if the mesh needs to be highly deformed to fit inside the component geometry, in some points where the material will not be really stressed, some triangular elements can be chosen to help in making the mesh as less deformed as possible.

4.2.3 Solid elements

In the case of solid elements, they can also be defined with different numbers of nodes. Typically, these elements are available in four-node and eight-node configurations, though higher-order elements with more nodes, such as 10 or 20 nodes, are also common.

Four-node solid elements, that are tetrahedral elements, have linear shape functions in both directions. Like three-node elements in 2D elements, the stress is assumed to be constant within the element. However, their stiffness is generally higher than that of the higher number of nodes elements. These elements are widely used in solid mechanics problems, especially when meshing is structured, and they provide a reasonable balance between accuracy and computational efficiency.

Eight-node solid elements, that are basic hexahedral elements, are the most commonly used in solid mechanics analysis due to their accuracy and ability to handle complex stress distributions. Their shape functions are quadratic, which allows for a more refined approximation of the displacement field within the element. This leads to a better representation of the stress gradients inside the element. Eight-node elements are well-suited for simulations that require high accuracy, especially in the case of non-linear material behavior or where stress concentrations are significant.

Higher-order solid elements (up to 27 nodes) offer even more accurate results by introducing additional nodes for more complex shape functions. These elements are used in highly detailed analyses or where the material behavior is highly non-linear, increasing the number of nodes, the stress distribution inside the element is

described with higher order functions.

Generally an analysis with solid elements uses hexaedral elements, using tet-elements only when required when the hex-elements will excessively deform the mesh.

4.3 LS-Dyna

LS-Dyna is a commercial FEA software commercialized from Ansys, Inc., an American multinational company that develops and market CAE software's. LS-Dyna was firstly developed from Livermore Software Technology Corporation (LSTC). The first software, Dyna3D, that is the predecessor of LS-Dyna software, was developed to simulate the impact of the FUFO bomb dropped from a low altitude and an impact velocity ~40 m/s. In 1976 the first manual have been published, and in 1978 the first sourced code have been published for public domain. LSTC decided than to concentrate in developing a code that was capable to combine different solvers and solve multi-physics problems. *"Combine multi-physics capabilities in a scalable code for solving highly nonlinear transient problems to enable the solution of coupled multi-physics and multi-stage problems in one run [16]".* In 2019 Ansys acquired the software from LSTC.

Explicit vs. Implicit

In LS-Dyna it is possible to use both an implicit or an explicit solver, and it is also possible to jump between the two type of solvers. The main difference between explicit and implicit time step scheme is that the explicit scheme is conditionally asymptotically stable while the implicit scheme is unconditionally asymptotically stable. This mean that the timestep can be decided unconditionally only with the implicit solver. Nevertheless, the explicit Euler scheme is the one that is most used in FE analysis for crash simulations and to simulate non linearity. This because an implicit solver works very well if the time step chosen is wide, while in case of non linearity or crash, it's useful to have a smaller time step to better follow the non linearity. For each iteration the calculation time is lower when using an explicit solver, for this reason the explicit solver is used in the cases where the brevity of time step is important for the solution of the problem.

4.4 Finite element models

With the experimental data obtained, a numerical model in LS-Dyna® of the materials have been developed. To do that, some simulation have been performed, starting from a single element simulation, passing through the ASTM specimen

geometries and finishing with a simulation of a real component. After some attempts, the material card chosen to better simulate the material behavior have been the material card MAT_058 available in LS-Dyna® software.

4.4.1 MAT 54: Enhanced Composite Fabrics

Material card MAT_054 in Ls-Dyna® is a very accurate card that describe linear behavior of composites. This type of material card use the Chang-Chang failure criterion. To fully describe the behavior of the material, the following data have been input:

- Direction A and B young moduli
- AB, AC, BC Poisson ratios
- Maximum stress in A and B direction of the material both in tensile behavior and in compression behavior and and AB maximum shear stress
- Strain at failure of matrix, compressive and tensile fiber strain at failure and shear strain at failure
- Material density, evaluated as the weighted average density of fibers and matrix densities
- Global or local direction due to the orthotropicity of composite material

The directions cited in the list here above, are the one explained in figure 4.3, with A as principal direction, that usually is the one with better material properties, but in our case the 0 and 90° direction have the same properties.

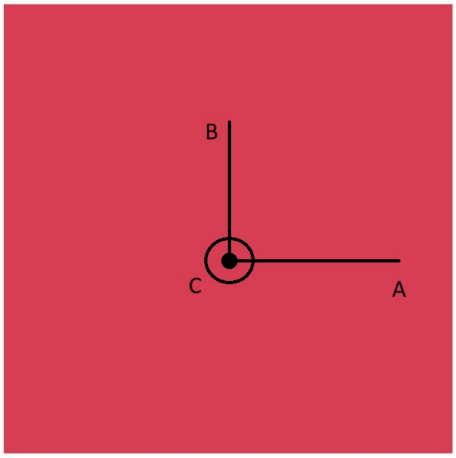

Figure 4.3: Material directions in the element

For sake of completeness, the density evaluation is reported. To do that, it is necessary to start by the single reinforcement material volume fraction

Table 4.2: Fibre and matrix volume fraction

Volume fraction	**Flax**	**Glass**
Fiber	33.92%	36.77%
Matrix	66.08%	63.23%

The weighted density have been evaluated with the rule of mixture, as reported at page 20/77 of the slides [17].

$$\rho_c = \rho_m V_m + \rho_f V_f$$

In this simulations two material cards have been created:

- MAT_54 Flax lamina
- MAT_54 Glass lamina

These material cards have been created in LS-Dyna ® using the data obtained during experimental results, reported in the figures 3.16. The various input of the cards have been modified using a single element simulation first of all and than simulating the entire specimens.

MAT_54 Flax

Table 4.3: Flax material card

TITLE	Flax fiber lamina						
MID	**RO**	**EA**	**EB**	**(EC)**	**PRBA**	**(PRCA)**	**(PRCB)**
1	1.232E-06	11.5	11.5	0.0	0.05	0.0	0.0
GAB	**GBC**	**GCA**	**(KF)**	**AOPT**	**2WAY**	**TI**	
1.9	1.9*	1.9*	0.0	2.0	1.0	0.0	
XP	**YP**	**ZP**	**A1**	**A2**	**A3**	**MANGLE**	
0.0	0.0	0.0	1.0	0.0	0.0	0.0	
V1	**V2**	**V3**	**D1**	**D2**	**D3**	**DFAILM**	**DFAILS**
0.0	0.0	0.0	0.0	0.0	0.0	0.2	0.041
TFAIL	**ALPH**	**SOFT**	**FBRT**	**YCFAC**	**DFAILT**	**DFAILC**	**EFS**
1.0e-06	0.0	0.85	0.0	2.0	0.35	-0.8	0.0
XC	**XT**	**YC**	**YT**	**SC**	**CRIT**	**BETA**	
0.08	0.114	0.08	0.114	0.038	54.0	0.32	
PEL	**EPSF**	**EPSR**	**TSMD**	**SOFT2**			
0.0	0.0	0.0	0.0	0.85			
SLIMT1	**SLIMC1**	**SLIMT2**	**SLIMC2**	**SLIMS**	**NCYRED**	**SOFTG**	
0.0	0.0	0.0	0.0	0.0	0.0	1.0	

MAT_54 Glass fiber

Table 4.4: Glass material card

TITLE	Glass fiber lamina						
MID	**RO**	**EA**	**EB**	**(EC)**	**PRBA**	**(PRCA)**	**(PRCB)**
1	1.620E-06	18.5	18.5	0.0	0.067	0.0	0.0
GAB	**GBC**	**GCA**	**(KF)**	**AOPT**	**2WAY**	**TI**	
3.9	3.9*	3.9*	0.0	2.0	1.0	0.0	
XP	**YP**	**ZP**	**A1**	**A2**	**A3**	**MANGLE**	
0.0	0.0	0.0	1.0	0.0	0.0	0.0	
V1	**V2**	**V3**	**D1**	**D2**	**D3**	**DFAILM**	**DFAILS**
0.0	0.0	0.0	0.0	0.0	0.0	0.2	0.04
TFAIL	**ALPH**	**SOFT**	**FBRT**	**YCFAC**	**DFAILT**	**DFAILC**	**EFS**
1.0e-06	0.0	0.85	0.0	2.0	0.35	-0.8	0.0
XC	**XT**	**YC**	**YT**	**SC**	**CRIT**	**BETA**	
0.224	0.224	0.224	0.224	0.063	54.0	0.32	
PEL	**EPSF**	**EPSR**	**TSMD**	**SOFT2**			
0.0	0.0	0.0	0.0	0.85			
SLIMT1	**SLIMC1**	**SLIMT2**	**SLIMC2**	**SLIMS**	**NCYRED**	**SOFTG**	
0.0	0.0	0.0	0.0	0.0	0.0	1.0	

- *: Values marked with two asterisks (*) are estimated. These values were not measured during experimental tests or are not available in TDS.

4.4.2 PART_COMPOSITE

In LS-Dyna ®it is possible to build the layup of the laminate using the PART_COMPOSITE instead of the normal part. Part composite works only with shell elements, it needs some inputs

Table 4.5: Example of $[GF]_{4s}$ PART COMPOSITE input

TITLE							
T2							
PID	ELFORM	SHRF	NLOC	MAREA	HGID	ADPOPT	THSHEL
2	16	0.83	0	0	0	0	0
MID1	THICK1	B1	TMID1	MID2	THICK2	B2	TMID2
2	0.175	0	0	1	0.61	0	0
2	0.175	0	0	1	0.61	0	0
1	0.61	0	0	2	0.175	0	0
1	0.61	0	0	2	0.175	0	0

The shear factor used is the default one, that is the results of rounding $\frac{5}{6}$. The element chosen are the default thin shell elements of LS-Dyna® that are fully integrated.

Because all the specimen have been tested only along 0° direction of the fabrics, only this direction have been replied in specimens, as it is possible to see in the columns B1 and B2 of the table 4.5.

4.4.3 Single element

For this simulation a shell element with dimensions 5x5 (that are mm because of the Units of measurements chosen).

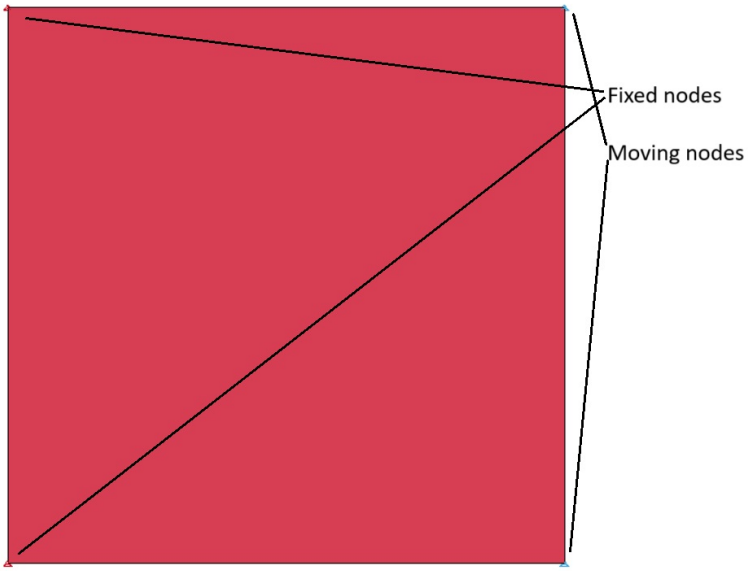

Figure 4.4: One element geometry to test the material card

For each stuck up sequence, the single element have been stretched in the three ways reported in figure 4.5, even if the expected final curve of each stuck up sequence should not change. After the simulation, the curves have been compared with the plots obtained during experimental campaign and some input have been changed. The simulation time of those three initial conditions, with one element only, is less than 1 second on an average laptop, that's why it has been possible to simulate it some times to correct one input a time.

(a) Element at the begin of the simulation

(b) Deformed element after shear deformation

(c) Deformed element after tensile deformation

(d) Deformed element after compressive deformation

Figure 4.5: Deformed elements at the end of the simulations

In figure 4.6 the comparison between experimental and numerical curves of tensile, compressive and shear are reported after the material card optimization.

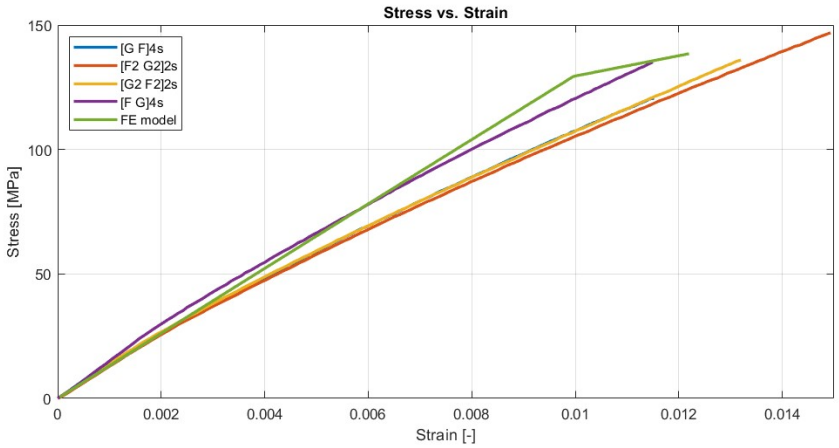

(a) tensile curves

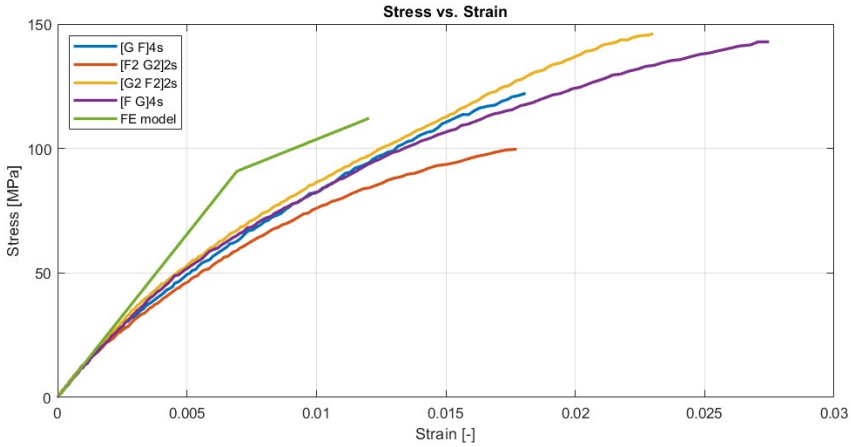

(b) compressive curves

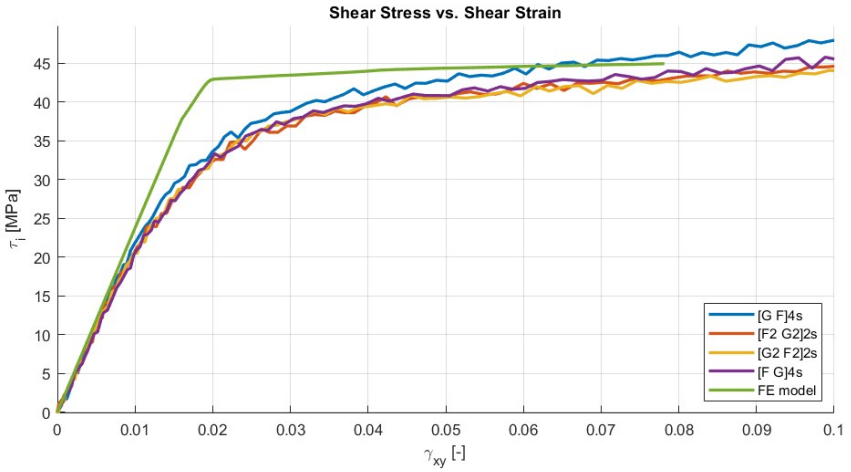

(c) Shear curves

Figure 4.6: Tensile, compressive e shear curves of the one element simulation

With the material cards reported in tables 4.3 and 4.4, the difference in percentage of the moduli are reported in table 4.6

Table 4.6: Young and shear moduli difference between experimental and numerical results

LAYUP	**Tensile**	**Compressive**	**Shear**
$[GF]4s$	0.50%	2.56%	2.32%
$[F2G2]2s$	5.32%	6.97%	5.83%
$[G2F2]2s$	2.00%	1.27%	7.81%
$[FG]4s$	7.06%	12.8%	12.66%

4.4.4 Specimen simulation

After tuning all the simulation parameters related to the material, the specimen have been simulated. The full specimen geometry have been reproduced and for each specimen the length of the part of the specimen have been chosen by fitting the maximum displacement with the maximum displacement of the real specimen. When the boundary conditions have been fitted, the force vs. displacement curves have been obtained and compared with the experimental curves. The chosen length between the node where the boundary conditions is set as the free length imposed from the Universal Testing Machine during the experimental tests, in this way the fracture occur at the same displacement of the boundary nodes and the cross-head of the machine.

Tensile test simulations

Tensile specimen have been simulated with a mesh of 1 x 1 mm, thanks to the geometry, all the elements are perfect squares with no deformed elements. The total number of elements of each simulation is 6250.

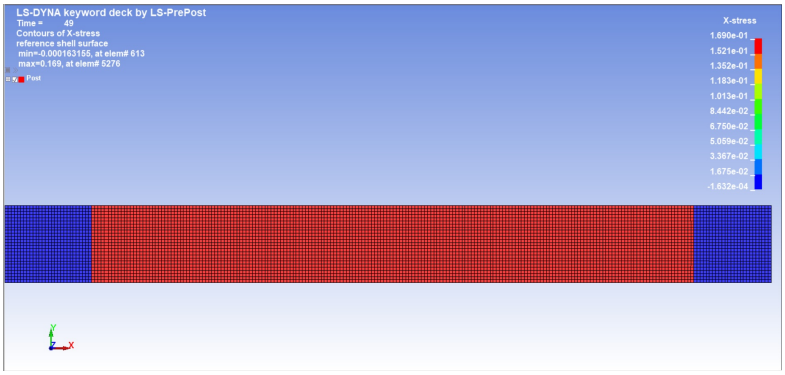

Figure 4.7: Tensile specimen FE model

In figure 4.7 it is possible to see that during the simulation the level of stress is distributed along the specimen equally, that is the reason why the ASTM standard decide this shape for the tensile specimen. During the simulation the specimen is perfectly straight, for this reason the breakage can start everywhere inside the gauge length, that is the area with red elements in figure 4.7.

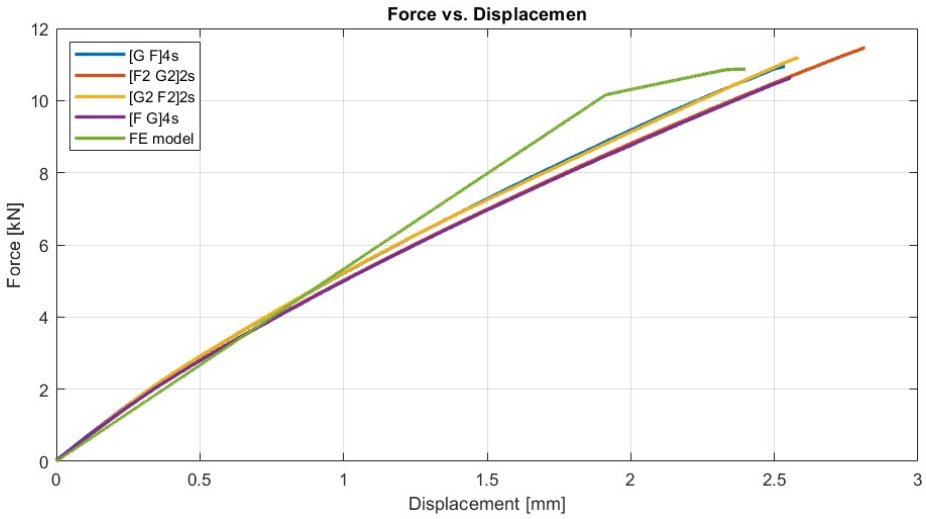

Figure 4.8: Force vs. displacement comparison between experimental curves and FEM curve

In figure 4.8 it is possible to see that the specimen behave in a very similar way in the first linear behavior of the material, after that it becomes more stiffer, that is something we expect looking at 4.6a

Compressive specimen

The compressive behavior is a bit less precise than the others, the specimen is a bit stiffer, but that's due to the fact material card 54 has as input only one young modulus and the material resulted a bit less stiff while loaded in compression. Also this specimen has 1 x 1 mm non distorted elements, for a total of 2000 elements.

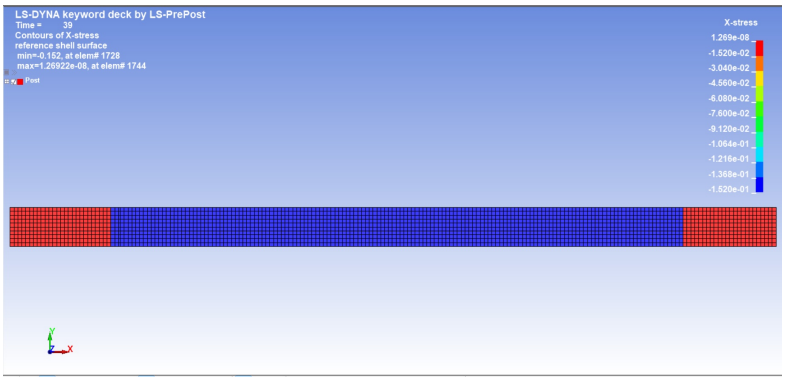

Figure 4.9: Compressive specimen FE model

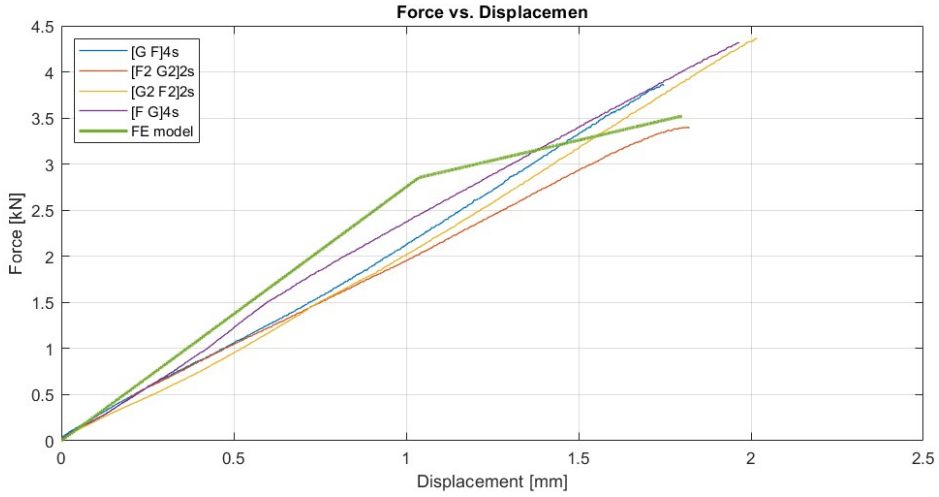

Figure 4.10: Force vs. displacement comparison between experimental curves and FEM curve

Iosipescu specimen

In the case of the shear specimen, the geometry is a bit more complicated. The dimension of the two sides of the specimen, where the load is applied, is reduced to

save the amount of elements tested, also because the load i this area has not been analyzed even during the experimental campaign. The total number of element is 2758, whit an average element dimension of 0.5 x 0.5 mm.

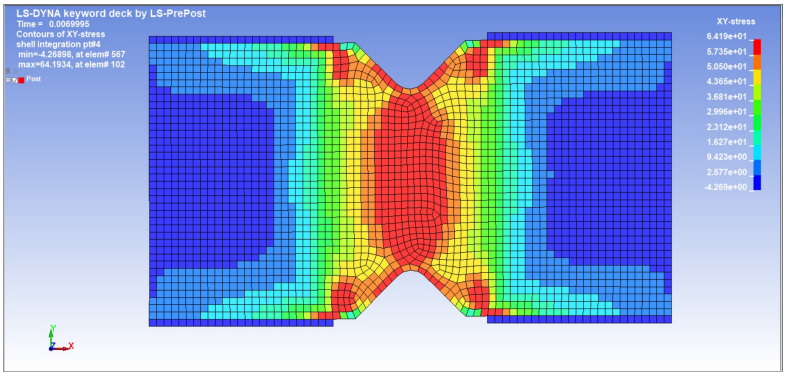

Figure 4.11: Compressive specimen FE model

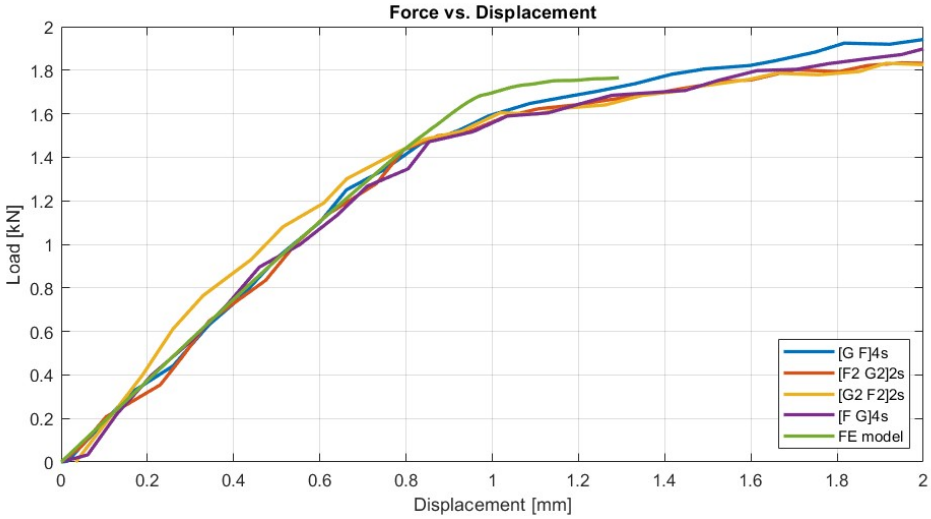

Figure 4.12: Force vs. displacement comparison between experimental curves and FEM curve

With the FE models curves reported in figures 4.8, 4.10 and 4.12 we can confidently say that the material card will behave in a similar way to the reality also if the simulated geometry is a real part.

Chapter 5

Design of an automotive crash absorber with hybrid materials

5.1 Part description

The material cards built have been used to simulate a real component and compare the mechanical properties of the layups. The component chosen is a impact attenuator for a formula SAE car, described in the article [18], where the component have been built and simulated with a carbon-epoxy prepreg material. The articles report the curves obtained during the experimental campaign and the curves obtained with a simulation in LS-Dyna®. The curves reported to describe the impact attenuator behavior are the Force vs. Displacement, reported in figure 5.1a and the curve that reports the deceleration of the impact plate in time, figure 5.1b.

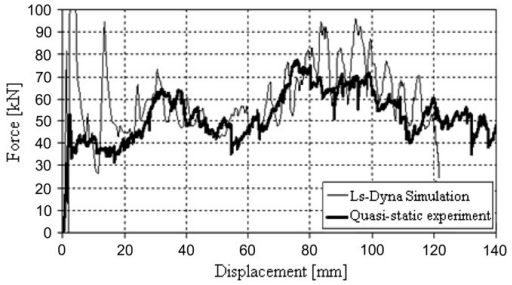

(a) Force vs. Displacement of the impact attenuator of the paper

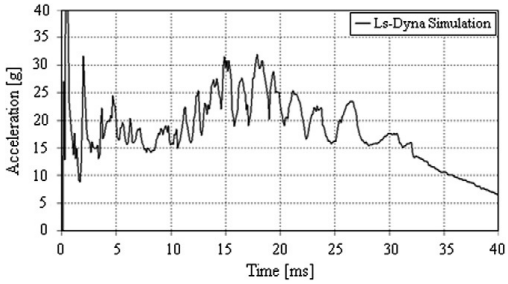

(b) Shear results for glass laminate

Figure 5.1: Deceleration vs. time of the impact attenuator of the paper

In the paper it is also reported a figure of the the crash simulation of the impact attenuator and a figure of the tested part, reported in figure 5.2, where it is possible to comprehend how the geometry is supposed to fail.

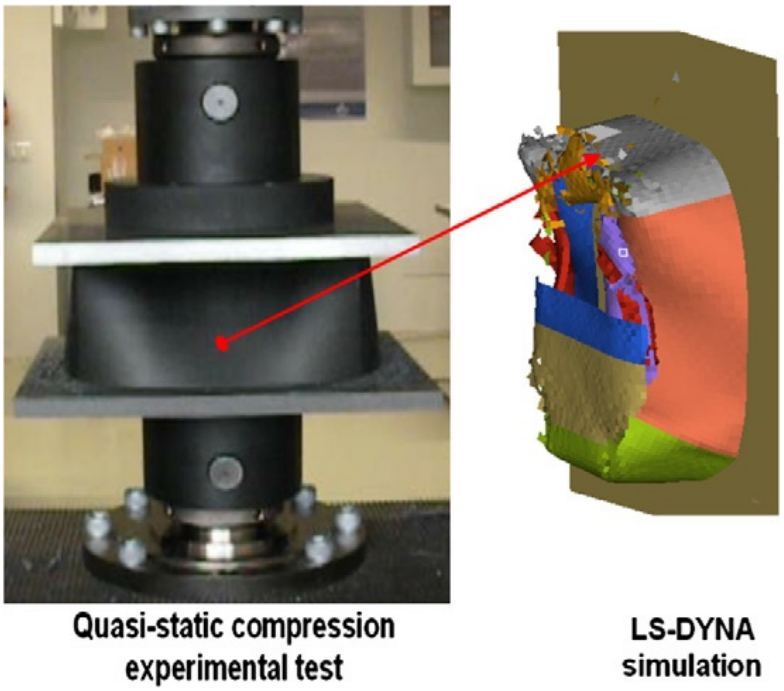

Figure 5.2: Experimental and numerical figure of the crashed impact attenuator

It is possible to notice that the structure collapses inward into the geometry. The same behavior is expected in the simulation with the Hybrid composite material.

5.2 Hybrid composite geometry simulation

The objective of the simulation is obtaining comparable curves, having a layup that reduce as much as possible the weight of the component, but having at least the 50% of the plies made with Flax fiber fabrics and that the layup is symmetric. The geometry simulated is exactly the same of the component of the paper and it has been reported in figure 5.3a.

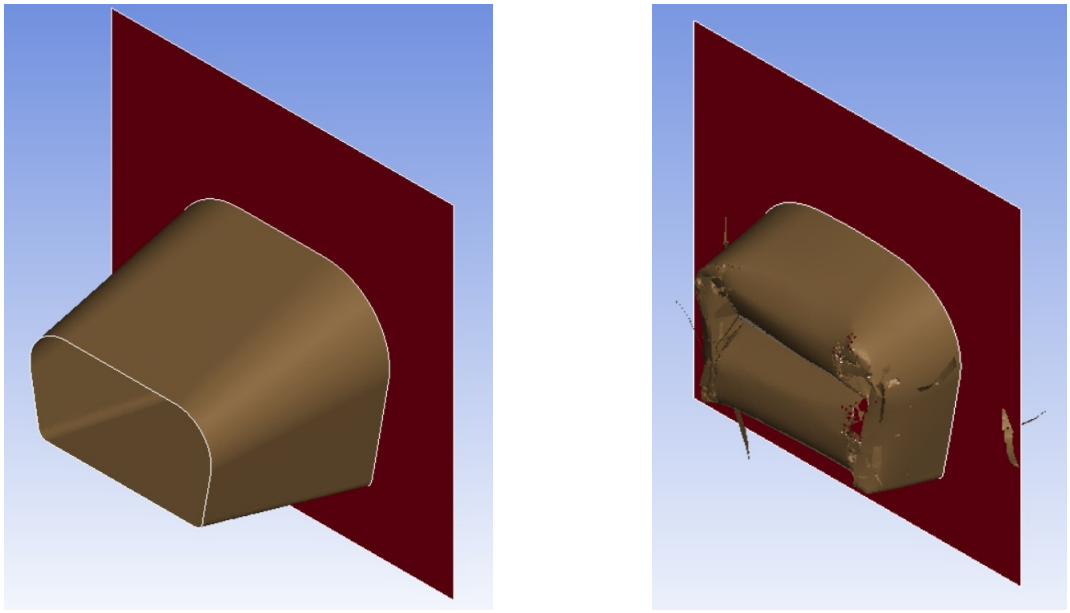

(a) Simulated geometry of the crash-box **(b)** Crashed geometry

Figure 5.3: Simulated geometries before and after crash

5.2.1 Iteration for layup optimization

Starting from the layup of the plates, the number of layers have been increased each simulation until reaching the minimum number of layers that dissipate all the energy that the impact wall has before crashing onto the component. As mentioned before, every simulation run has been done with a symmetric layup and a minimum of 50% of the layers made out of flax. The final amount of layers needed for each layup is 14, with 6 layers of glass fibers and 8 layers of flax fibers.

Table 5.1: Layup simulated

Layup n°	Extended layup notation	Short layup notation
1	[F/G/F/G/F/G/F/F/G/F/G/F/G/F]	[[F G]3 F]s
2	[F/F/F/G/G/G/F/F/G/G/G/F/F/F]	[F3 G3 F]s
3	[G/G/G/F/F/F/F/F/F/F/F/G/G/G]	[G3 F4]s
4	[G/F/G/F/G/F/F/F/F/G/F/G/F/G]	[[G F]3 F]s

The weight of the final geometry evaluated from LS-Dyna ® is around 1.2 kg, against the 0.62 kg of the carbon fiber layup. The curves obtained from the simulations are three, deceleration vs. time, force vs. displacement and the energy

vs displacement. This last curve has been added to verify that the total energy absorbed from the geometry is the real amount, to verify if the simulation have been set up correctly and also to have a look if the geometry is absorbed regularly while the geometry crash. The curve of the four final layup, reported in table 5.1 are reported in figure 5.4, 5.5 and figure 5.6.

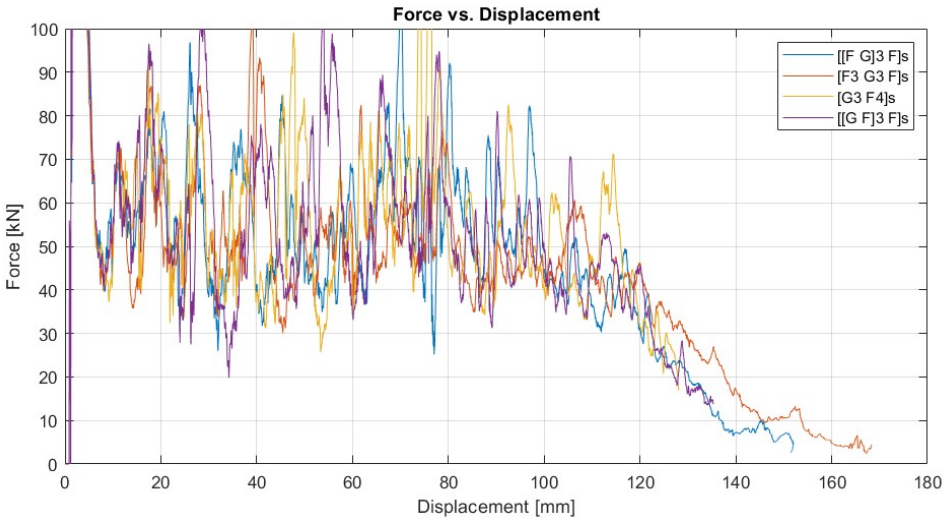

Figure 5.4: Force vs. Displacement curves

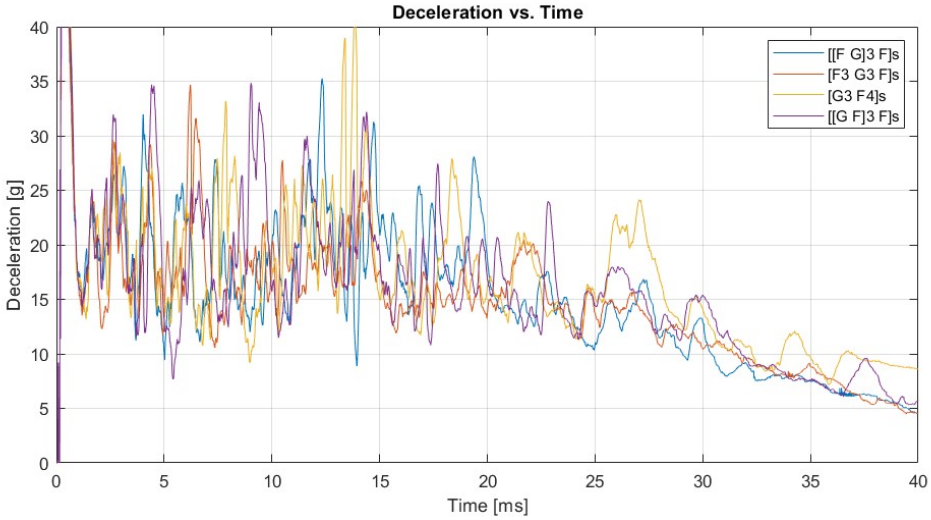

Figure 5.5: Deceleration vs. Time curves

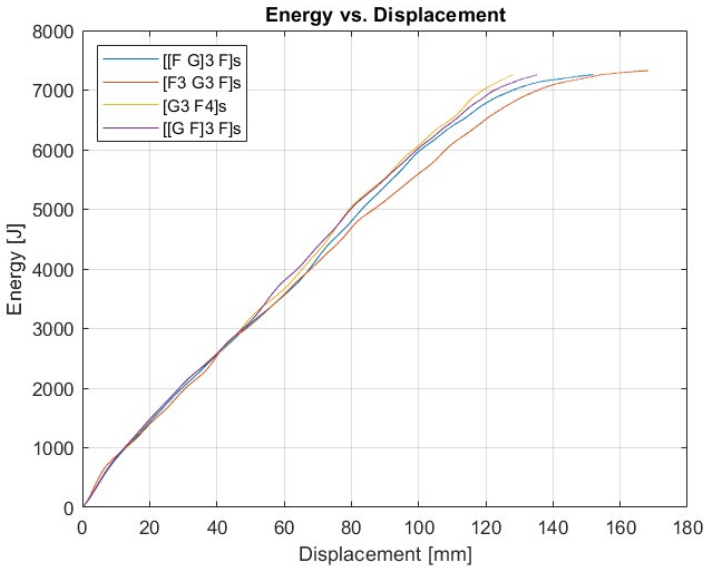

Figure 5.6: Energy vs. Displacement

The results obtained with the four different layups do not differ that much from each other, as it is possible to see from the plots. The only configuration that has something to notice is $[G3F4]s$, where it is possible to find some peaks of deceleration, and consecutively of force, while the component was crashing. In fact the average force and deceleration results to be the highest ones between all the other layups, even if $[[GF]_3F]s$ results are quite close. Because of the fact that the weight of the component in the four lay up is not changing, the best solution is the fourth configuration, where the layup is built by alternating a flax layer with a glass layer and where both outer layers are made of glass. The performance of the composite is increased by laminating the plies with outer layer made of glass, this because of the increment in the mechanical properties of the laminate in bending condition. The average results of the four layups are reported in table 5.4

Table 5.2: Results of the simulated component with the four Hybrid layup

Layup	Mass [kg]	Mean force [kN]	Mean acceleration [g]	Total Energy absorbed [J]	SAE [J/kg]
$[[FG]_3F]s$	1.163	23.70	8.05	7257	6240
$[F_3G_3F]s$	1.163	22.91	7.78	7327	6300
$[G_3F_4]s$	1.163	24.99	8.49	7257	6240
$[[GF]_3F]s$	1.163	24.95	8.48	7219	6207

5.2.2 Three Step layup

Starting from the weight obtained in the previous iteration, another iteration utilizing the layup scheme reported in the paper have been done. The iteration have been done trying to find out the way to dispose the thickness increment along the crash absorber having a weight as close as possible to the one obtained in the previous iteration. The three zones reported in figure 5.7 are long:

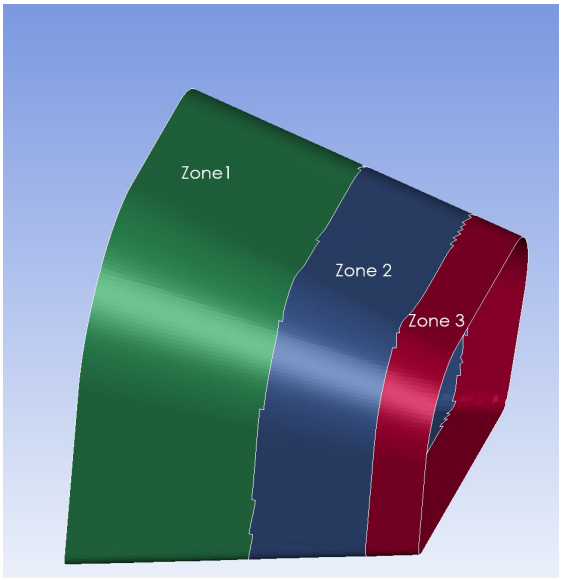

Figure 5.7: Zone distributions of the second iteration

- Zone 1: 100 mm
- Zone 2:70 mm
- Zone 3:30 mm

This is the same subdivision reported in the paper The four layup have been reproduced following table 5.3, for leaning the notation we will call them Layup 1-4 as reported in the same table.

Table 5.3: Layup of the second iterations, zone name reported as the ones in picture 5.7

Layup Name	Zone 1	Zone 2	Zone 3
Layup 1	[F/G/F/G/F/G/F/G/G/F/G/F/G/F/G/F]	[F/G/F/G/F/G/G/F/G/F/G/F]	[F/G/F/G/G/F/G/F]
Layup 2	[F/F/F/F/G/G/G/G/G/G/G/F/F/F/F]	[F/F/F/G/G/G/G/G/G/F/F/F]	[F/F/G/G/G/G/F/F]
Layup 3	[G/G/G/G/F/F/F/F/F/F/F/G/G/G/G]	[G/G/G/F/F/F/F/F/F/G/G/G]	[G/G/F/F/F/F/G/G]
Layup 4	[G/F/G/F/G/F/G/F/F/G/F/G/F/G/F/G]	[G/F/G/F/G/F/F/G/F/G/F/G]	[G/F/G/F/F/G/F/G]

As for the first iteration pattern, the curves of the lightest layup obtained are reported with the four layer deposition compared.

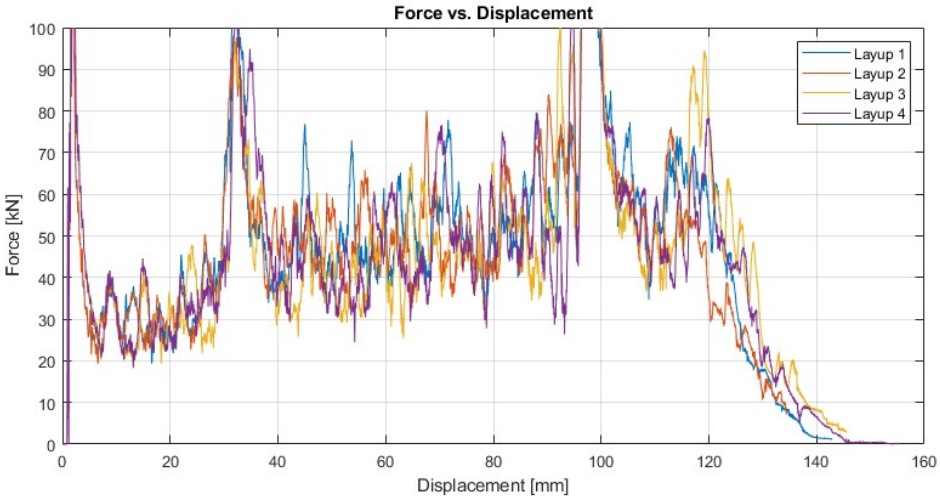

Figure 5.8: Force vs. Displacement curves

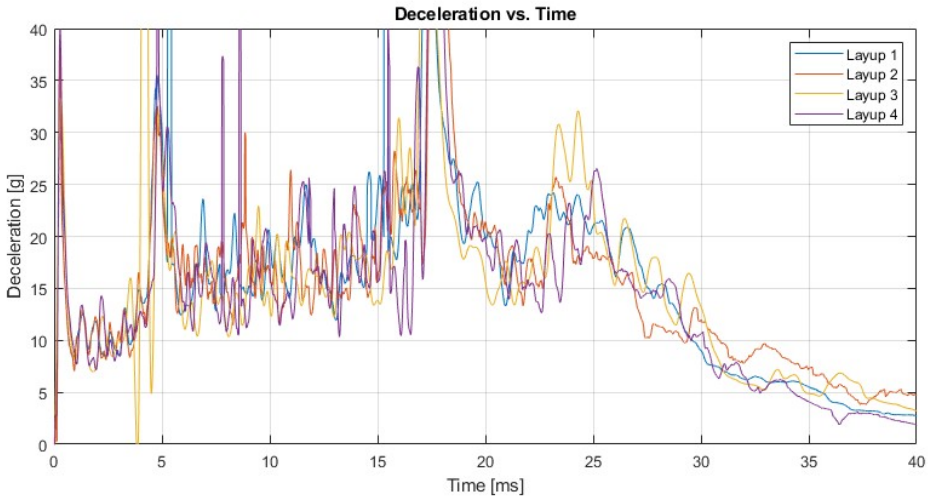

Figure 5.9: Deceleration vs. Time curves

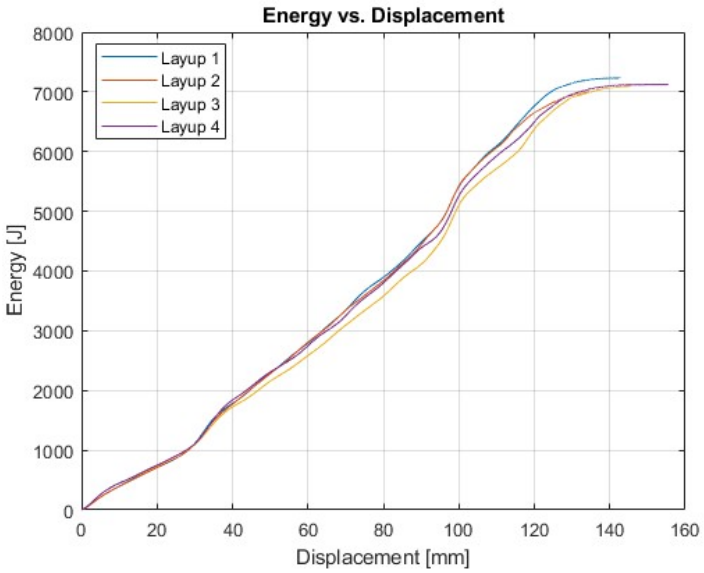

Figure 5.10: Energy vs. Displacement

The main difference that we can see if compared with the one thickness layup is that a huge amount of energy is absorbed from the last half of the component, while the rest of the component is breaking out without absorbing as much of energy.

This bring to have higher forces during the breakage and also an higher average deceleration, as it is possible to notice from results, reported in table **??**.

Table 5.4: Results of the simulated component with the four Hybrid layup

Layup	Mass [kg]	Mean force [kN]	Mean acceleration [g]	Total Energy absorbed [J]	SAE [J/kg]
Layup1	1.078	33.22	11.59	7032	6523
Layup2	1.078	35.22	11.98	7001	6494
Layup3	1.078	33.36	11.85	7096	6583
Layup4	1.078	30.99	10.68	7123	6608

Also in this case the different layup report results that are very similar each other, but it is possible to notice how in energy absorption per unit of mass the two layups with outer glass layers perform better.

5.3 Results

All the simulated layup result report that they are a good compromise between the increment of weight and having at least 50% of the component manufactured with Bio based materials. The final weight is always less then twice the carbon fiber made component, that it is also interesting to remember the fact that the volume content of fibers was higher. The simulated component report very similar amount of energy dissipated per unit of mass and all of them are higher then half of the energy that carbon fiber component can absorb. The total results are reported for sake of simplicity in a unique table 5.5.

Table 5.5: Results of the simulated component with the four Hybrid layup

Layup	Mass [kg]	Mean force [kN]	Mean acceleration [g]	Total Energy absorbed [J]	SAE [J/kg]
$[[FG]_3F]s$	1.163	23.70	8.05	7257	6240
$[F_3G_3F]s$	1.163	22.91	7.78	7327	6300
$[G_3F_4]s$	1.163	24.99	8.49	7257	6240
$[[GF]_3F]s$	1.163	24.95	8.48	7219	6207
Layup1	1.078	33.22	11.59	7032	6523
Layup2	1.078	35.22	11.98	7001	6494
Layup3	1.078	33.36	11.85	7096	6583
Layup4	1.078	30.99	10.68	7123	6608
CF	0.62	40.30	13.70	7041	11356

Despite the simulation results of three step version of the component, there are some peculiarity that have to be taken into account. First of all, no test have been done to simulate the behavior of this hybrid composite in the plies overlap regions. This discontinuity in the tow can generate localized stresses and this can bring to a lower force failure of the crash-box making some zone not dissipating all the energy they could have. This reason can be connected with the second point that is the difference in weight between single thickness version and three zones version, which is less than 10%, this difference can be further decrease taking into account the overlaped material. Last consideration to be done is the fact that this thicker regions can cause spikes in the impact force and also being weaker in the first zone the force is higher at the end of the energy dissipation, where velocities are lower but it is also necessary to take into account that this forces are more easily transferred to the rest of the structure since the shorter the crash absorber become, less compliant the structure is. All this considerations can be changed in case of a

further campaign to investigate overlap behavior of this hybrid composites.

Conclusions

The aim of this thesis is to analyses a possible alternative to conventional composite material and how to decrease as much as possible the loss of mechanical properties. Hybridization of fiber composites is a promising approach to consider when the goal is to reduce the carbon footprint of a component while minimizing the reduction in its mechanical properties. Although the performance does not yet match that of prepreg composite materials cured in an autoclave, the components simulated in this thesis demonstrate feasible weight and thickness characteristics for real-world applications.

In case of producing an hybrid composite component there are further things to think about when deciding the layup. From the results obtained it should be ideal to design an hybrid composite with the lamina that has the higher mechanical properties as outer ply.

Because of the fact that material properties of the full laminate are decreased, it is necessary to design components increasing the thickness, this mean that it is possible that the mold of a component should be manufactured again to adapt with new dimensions.

The material properties of the hybrid composites are decreased by 44% in the worst case, that is the shear moduli of the configuration $[FG]_{4s}$ up to only a 26% less in the tensile Young moduli of the same layup. Comparing the maximum stresses, the highest loss is the maximum tensile stress of the layup $[GF]_{4s}$ with 42 % of decrement in the σ_{UTS} while the minimum loss is the maximum shear stress of the stacking sequence $[FG]_{4s}$ with a loss around 29%.

With the numerical model is possible to predict the behavior of the component that will be designed with this hybridization and it is possible to predict the behavior also changing the layup and the number of layers, having the same material card for each lamina and the results obtained do not differ more than 5% in almost all the different test reproduced in LS-Dyna®.

This thesis represents an initial step toward assessing the feasibility of using hybrid composites as an alternative to single-fiber composites. Further research can expand on these findings through additional experimental campaigns, exploring different layup configurations. This could include varying ply orientations by

introducing 30° and 45° angle shifts and in both cases going through all the ply sequence as done in this thesis, to analyze how these changes influence the overall behavior of the material. Such studies would provide deeper insight into the interaction between flax and E-glass fibers and help determine whether specific configurations can enhance shear properties. Another interesting campaign is doing the same experimental campaign with exactly the same material but pre-impregnating the tows, to decrease the amount of resin, and curing the laminate in autoclave with pressure, this will for sure the material properties of the hybrid laminates and probably decrease the difference in weight and thickness between the component made of carbon fiber-epoxy resin composite and the same component with the hybrid composites. The reduction in weight will be obtained for sure decreasing the resin amount, but also there is the possibility that less plies should be used for having the same amount of mechanical properties. In case a prepreg campaign will be performed, a very interesting comparison about voids percentage can be performed by CT scanning the specimen before testing. Because of the high moisture absorption of flax fibers, another plate can be manufactured and the same experimental campaign can be performed after an aging process is done on the cut specimen, since the final components edges should be post processed and creates the same edge nature as a water-jet cut or a diamond blade.

Based on the data obtained during this thesis work, we can conclude that hybridization offers a promising approach for reducing the carbon footprint of composite materials, without significantly compromising the mechanical properties of the final component. The results indicate that carefully engineered hybrid composites can balance sustainability with performance, making them a viable option for environmentally-conscious material design. However, further studies are necessary to gain a deeper understanding of the long-term behavior and overall performance of these materials.

Bibliography

[1] Rahul Reddy Nagavally. «Composite Materials - History, Types, Fabrication Techniques, Advantages, and Applications». In: *International Journal of Mechanical and Production Engineering* 5.9 (2017). E-mail: rahulnagavally@gmail.com, pp. 82–87 (cit. on p. 1).

[2] Aliakbar Gholampour and Togay Ozbakkaloglu. «A review of natural fiber composites: properties, modification and processing techniques, characterization, applications». In: *Springer Science+Business Media, LLC* 830 (Sept. 2019), pp. 830–831 (cit. on p. 4).

[3] Alejandra Gomez-Campos, Claire Vialle, Antoine Rouilly, Caroline Sablayrolles, and Lorie Hamelin. «Flax Fiber for Technical Textile: A Life Cycle Inventory». In: *Laboratoire de Chimie Agro-industrielle, LCA, Université de Toulouse, INRAE, Toulouse, France; Toulouse Biotechnology Institute (TBI), INSA, INRAE UMR792 and CNRS UMR5504, Federal University of Toulouse, Toulouse, France* (2020). Available upon request from corresponding authors (alejandra.gomezcampos@ensiacet.fr, claire.vialle@ensiacet.fr). DOI: 10.1016/j.jclepro.2020.125177 (cit. on p. 5).

[4] Davide Salvatore Paolino. *Lecture n. 3 – Lamina failure*. Slide of the course A.Y. 2022-2023. 2022 (cit. on p. 8).

[5] Delprete C., Firrone C., Rosso C., and Somà A. *Fondamenti di Meccanica Strutturale*. Levrotto & Bella, 2013 (cit. on p. 10).

[6] Antigoni Barouni, Colin Lupton, Chulin Jiang, Abu Saifullah, Khaled Giasin, Zhongyi Zhang, and Hom N. Dhakal. «Investigation into the fatigue properties of flax fibre epoxy composites and hybrid composites based on flax and glass fibres». In: *Composite Structures* 281.10 (Dec. 2021). DOI: 10.1016/j.compstruct.2021.115046 (cit. on pp. 11, 12).

[7] J.L. Liu et al. «Improving the impact performance of natural fiber reinforced laminate through hybridization and layup design». In: *Composites Science and Technology* 245 (2024), p. 110585. DOI: 10.1016/j.compscitech.2024.110585 (cit. on pp. 13, 14).

[8] A.W. Van Vuure, J. Baets, K. Wouters, and K. Hendrickx. «Compressive properties of natural fibre composites». In: *Materials Letters* 149 (2015), pp. 138–140. DOI: 10.1016/j.matlet.2015.01.158. URL: https://doi.org/10.1016/j.matlet.2015.01.158 (cit. on p. 13).

[9] Chandresh Vyas & R L Jhala. «Mechanical Characterization of Glass-Basalt Hybrid Composites with Different Fiber Weight Fraction». In: *Mechanics of Composite Materials* 11.2 (Apr. 2024), pp. 295–308. DOI: 10.22075/MACS.2024.31330.1541 (cit. on pp. 15, 16).

[10] ASTM International. *Standard Test Method for Tensile Properties of Polymer Matrix Composite Materials*. ASTM D3039/D3039M - 20. Available from ASTM International, 100 Barr Harbor Drive, West Conshohocken, PA 19428-2959, USA. 2022. URL: https://www.astm.org/Standards/D3039.htm (cit. on pp. 18, 40).

[11] ASTM International. *Standard Test Methods for Flexural Properties of Unreinforced and Reinforced Plastics and Electrical Insulating Materials*. ASTM D790 - 21. Available from ASTM International, 100 Barr Harbor Drive, West Conshohocken, PA 19428-2959, USA. 2021. URL: https://www.astm.org/Standards/D790.htm (cit. on p. 19).

[12] *ASTM D695-15: Standard Test Method for Compressive Properties of Rigid Plastics*. West Conshohocken, PA: ASTM International, 2015. URL: https://www.astm.org/Standards/D695 (cit. on pp. 19, 42).

[13] *ASTM D5379-19: Standard Test Method for Shear Properties of Composite Materials by the V-Notched Beam Method*. West Conshohocken, PA: ASTM International, 2015. URL: https://www.astm.org/Standards/D5379.htm (cit. on pp. 20, 44).

[14] Raffaele Ciardiello. *Design of lightweight and composite structures: Strain Gauges (or gages). Tutorial 2, Department of Mechanical and Aerospace Engineering, Politecnico di Torino*. Accessed: 21/03/2023. 2023 (cit. on pp. 24–31).

[15] Aurelio Soma. *Lezione n. 1 – Introduzione al corso*. Slide of the course A.Y. 2022-2023. 2022 (cit. on p. 50).

[16] David J. Benson. *The History of LS-DYNA®*. Department of Mechanical and Aerospace Engineering, UCSD. Accessed: [your access date here] (cit. on p. 54).

[17] Davide Salvatore Paolino. *Lecture n. 2 – Micromechanics*. Slide of the course A.Y. 2022-2023. 2022 (cit. on p. 56).

[18] Jovan Obradovic, Simonetta Boria, and Giovanni Belingardi. «Lightweight design and crash analysis of composite frontal impact energy absorbing structures». In: *Composites Part B: Engineering* 43.10 (2012). DOI: 10.1016/j.compositesb.2012.06.006 (cit. on p. 66).